

Cell competition acts as a purifying selection to eliminate cells with mitochondrial defects during early mouse development

Ana Lima^{1,2,#}, Gabriele Lubatti^{3,4,5,#}, Jörg Burgstaller⁶, Di Hu⁷, Alistair Green⁸, Aida Di Gregorio¹, Tamzin Zawadzki¹, Barbara Pernaute^{1,9}, Elmir Mahammadov^{3,4,5}, Salvador Perez Montero¹, Marian Dore², Juan Miguel Sanchez¹, Sarah Bowling¹, Margarida Sancho¹, Mohammad Karimi^{2,10}, David Carling², Nick Jones⁸, Shankar Srinivas⁷, Antonio Scialdone^{3,4,5,11,*} and Tristan A. Rodriguez^{1,11,*}

¹ National Heart and Lung Institute, Imperial College London, UK

² MRC London Institute of Medical Sciences (LMS), Institute of Clinical Sciences, Imperial College London, UK

³ Institute of Epigenetics and Stem Cells, Helmholtz Zentrum München, Munich, Germany

⁴ Institute of Functional Epigenetics, Helmholtz Zentrum München, Neuherberg, Germany

⁵ Institute of Computational Biology, Helmholtz Zentrum München, Neuherberg, Germany

⁶ Institute of Animal Breeding and Genetics, University of Veterinary Medicine, Vienna, Austria

⁷ Department of Physiology, Anatomy and Genetics, University of Oxford, Oxford, UK

⁸ Department of Mathematics, Imperial College London, UK.

⁹ Current address: Centre for Genomic Regulation (CRG), The Barcelona Institute of Science and Technology, Dr. Aiguader 88, Barcelona 08003, Spain

¹⁰ Current address: Comprehensive Cancer Centre, School of Cancer & Pharmaceutical Sciences, Faculty of Life Sciences & Medicine, King's College London, Denmark Hill, London SE5 9NU, UK.

¹¹ These authors jointly supervised this work.

Both these authors contributed equally

* Authors for correspondence: antonio.scialdone@helmholtz-muenchen.de;

tristan.rodriquez@imperial.ac.uk

Abstract

Cell competition is emerging as a quality control mechanism that eliminates unfit cells in a wide range of settings from development to the adult. However, the nature of the cells normally eliminated by cell competition and what triggers their elimination remains poorly understood. In mouse, prior to gastrulation 35% of epiblast cells are eliminated. Here we have performed single cell transcriptional profiling of these cells and find that they show the hallmarks of cell competition and have mitochondrial defects. We demonstrate that mitochondrial defects are common to a range of different loser cell types and that manipulating mitochondrial function is sufficient to trigger competition. Importantly, we show that in the embryo cell competition eliminates cells with mitochondrial DNA mutations and that even non-pathological changes in mitochondrial DNA sequence can induce cell competition. Our results therefore suggest that cell competition is a purifying selection that optimises mitochondrial performance prior to gastrulation.

Running title: Cell competition and mitochondrial selection

Keywords: mitochondria, mtDNA, mouse development, cell competition, purifying selection

1 Cell competition is a fitness sensing mechanism that eliminates cells that, although viable, are
2 less fit than their neighbours. The cells that are eliminated are generically termed losers, while
3 the fitter cells that survive are referred to as winners. Cell competition has been shown to act in
4 a broad range of settings, from the developing embryo to the ageing organisms¹⁻³. It has been
5 primarily studied in *Drosophila*, where it was first described in the imaginal wing disc⁴. Since
6 then, it has also been found to be conserved in mammals. In the mouse embryo 35% of
7 embryonic cells are eliminated between E5.5 and E6.5 and there is strong evidence that this
8 elimination is through cell competition⁵⁻⁷. These and other studies identified a number of read-
9 outs of cell competition in the mouse embryo, such as relative low c-MYC expression, a loss of
10 mTOR signalling, low TEAD activity, high P53 expression, or elevated levels of ERK
11 phosphorylation⁵⁻⁹. Importantly, there is a significant overlap with the markers of cell competition
12 originally identified in *Drosophila* as well as those found in other cell competition models, such
13 as Madin-Darby Canine Kidney (MDCK) cells – as reviewed¹⁻³. In spite of the advance that
14 having these cell competition markers signifies, given that they were primarily identified by using
15 genetic models that rely on over-expression or mutation, we still have little insight into the over-
16 arching features of the cells that are eliminated in the physiological context.

17 Mitochondria, with their diverse cellular functions ranging from determining the bioenergetic
18 output of the cell to regulating its apoptotic response, are strong candidates for determining
19 competitive cell fitness. During early mouse development mitochondria undergo profound
20 changes in their shape and activity¹⁰. In the pre-implantation embryo mitochondria are rounded,
21 fragmented and contain sparse cristae, but upon implantation they fuse to form complex
22 networks with mature cristae¹¹. The mode of replication of the mitochondrial genome (mtDNA),
23 that encodes for vital components of the bioenergetic machinery, also changes during early
24 mouse development. After fertilization, mtDNA replication ceases and its copy number per cell
25 decreases with every division until post-implantation stages, when mtDNA replication resumes¹⁰.
26 As the mutation rate of mtDNA is significantly higher than that of nuclear DNA^{12, 13}, this
27 increased replication most likely leads to an increased mutation load. In fact, inheritable mtDNA

28 based diseases are reported with a prevalence of 5-15 cases per 100,000 individuals^{14, 15}. A
29 number of mechanisms have been proposed to reduce this mutation load, such as the
30 bottleneck effect, purifying selection or biased segregation of mtDNA haplotypes¹⁶⁻²¹. However,
31 how these mechanisms act at the molecular and cellular level is still poorly understood.
32 To understand the nature of the cells eliminated during early mouse post-implantation
33 development, we have analysed their transcriptional profile by single-cell RNA sequencing and
34 found that these cells share a cell competition signature. Analysis of the pathways mis-regulated
35 identified mitochondrial dysfunction as a common feature. Importantly, our studies uncovered
36 that the cells eliminated have mtDNA mutations. Furthermore, we demonstrate that manipulating
37 mitochondrial activity either by disrupting mitochondrial dynamics or by introducing non-
38 pathological mtDNA changes is sufficient to trigger cell competition. These results therefore
39 pinpoint mitochondrial performance as a key cellular feature that determines the competitive
40 ability of embryonic cells and suggest that cell competition is acting as a purifying selection
41 during early mammalian development.

42

43 **Results**

44 **Cells eliminated in the early mouse embryo have a distinct transcriptional profile**

45 We have previously shown that in the early post-implantation mouse embryo about 35% of
46 epiblast cells are eliminated and that these cells are marked by low mTOR signalling⁷. However,
47 we currently do not understand the characteristics of these cells or what triggers their
48 elimination. To answer these questions, we have analysed their transcriptional profile by single
49 cell RNA sequencing (scRNA-seq). To ensure we can capture the eliminated cells, as we have
50 done before⁷, we isolated embryos at E5.5 and cultured them for 16 hours in the presence of a
51 caspase inhibitors (CI) or vehicle (DMSO) (Fig. 1a). Unsupervised clustering of the scRNA-seq
52 data revealed five clusters: two corresponding to extra-embryonic tissues (visceral endoderm
53 and extra-embryonic ectoderm) and three that expressed epiblast marker genes (Fig. 1b-c,
54 Extended Data Fig. 1a-f and Methods). Interestingly, cells from CI- and DMSO-treated embryos

55 are unequally distributed across the three epiblast clusters. In particular, one of these clusters
56 (cluster 4) is only composed of cells from CI-treated embryos (Fig. 1d-e). It is worth noting that
57 all epiblast clusters contained cells in G2/M and S phases of the cell cycle, suggesting they are
58 all cycling (Extended Data Fig. 2a).

59 The three epiblast clusters are highly connected, as highlighted by a connectivity analysis
60 carried out with PAGA²² (Extended Data Fig. 2b). Hence, to establish the relationship between
61 these epiblast clusters we computed a diffusion map²³. For this, we selected only cells captured
62 from CI-treated embryos, to eliminate possible confounding effects due to the caspase inhibitor
63 (Fig. 2a). However, when all epiblast cells are considered, the results remain unchanged
64 (Extended Data Fig. 2c-e). This analysis identified a trajectory between the three epiblast
65 clusters, with those cells unique to CI-treated embryos falling at one extreme end of the
66 trajectory (corresponding to cluster 4; Fig. 2a) and with those cells present in both DMSO and
67 CI-treated embryos at the other (corresponding to cluster 1; Fig. 2a and Extended Data Fig. 2d).

68 To further define the identity of the epiblast cells of CI-treated embryos we analysed the genes
69 differentially expressed along the trajectory (see Methods and Extended Data Fig. 3a) using
70 Ingenuity Pathway Analysis (IPA) to characterize gene signatures²⁴. Importantly, we found that
71 these differentially expressed genes fell under molecular and cellular function categories
72 associated with cell death and survival, protein synthesis and nucleic acids (Fig. 2b). Analysis of
73 the factors with enriched targets within the genes differentially expressed along the trajectory
74 revealed RICTOR (an mTOR component), TLE3, MYC, MYCN, P53 and IGFR (that is upstream
75 of mTOR) as the top upstream regulators (Fig. 2c). Breaking down the differentially expressed
76 genes into those down-regulated or up-regulated along the winner-to loser trajectory revealed
77 that the targets of RICTOR, MYC, MYCN and IGFR primarily fell within the down-regulated
78 genes (Supplementary Tables 1 and 2). P53 activated targets were preferentially up-regulated
79 and P53 repressed targets were preferentially down-regulated (Extended Data Fig. 3b-c).
80 Moreover, genes related to protein synthesis were primarily found to be downregulated.

81 The observation that the genes differentially expressed along the trajectory fall into cell death
82 categories, as well as being mTOR, MYC and P53 targets strongly suggests that cells at each
83 end of the trajectory are the winners and losers of cell competition⁵⁻⁷. For this reason, we
84 hereafter refer to those epiblast cells unique to CI-treated embryos as “loser” epiblast cells and
85 to those at the opposite end of the trajectory as the “winner” epiblast cells. Those cells lying
86 between these two populations on the trajectory are considered “intermediate”. Using this
87 knowledge we can define a diffusion pseudotime (dpt) coordinate²⁵ originating in the “winner”
88 cluster that tracks the position of cells along the trajectory and that can be interpreted as a
89 “losing score”, i.e., it quantifies how strong the signature of the “losing” state is in the
90 transcriptome of a cell (see Fig. 2d-e).

91 In accordance with previous studies^{6, 8, 9}, we also found evidence for miss-patterning in the
92 eliminated epiblast cells, as a proportion of these cells co-expressed naïve pluripotency and
93 differentiation markers (Fig. 2f and Extended Data Fig. 3d). To test if loser cells are
94 developmentally delayed or advanced compared to control cells we projected our data onto a
95 previously published diffusion map that includes epiblast cells from E5.5, E6.25 and E6.5 stage
96 embryos²⁶. We found that all epiblast cells, irrespective of the condition the embryos were
97 cultured in (ie, DMSO or CI-treated) and of their losing state (ie, that they belonged to the
98 winner, intermediate or loser cluster) mostly overlap with the E6.5 epiblast cells (Extended data
99 Fig. 3e-g). Cells from the loser cluster are slightly closer to the E6.25 stage than the winner and
100 intermediate cells, as shown by their pseudo-time coordinate, but they remain far from the earlier
101 E5.5 stage. This result combined with the higher expression of some differentiation markers
102 observed in loser cells suggests that these cells are miss-patterned rather than developmentally
103 delayed.

104 **Loser cells are characterised by defects in mitochondrial function**

105 We next analysed using IPA the cellular pathways mis-regulated in loser epiblast cells and found
106 that the top two pathways (mitochondrial dysfunction and oxidative phosphorylation) are related
107 to mitochondrial function (Fig. 3a-b, Supplementary Table 1 and 2). For example, we found a

108 down-regulation along the winner to loser trajectory of the mtDNA encoded *mt-Nd3* and *mt-Atp6*,
109 of regulators of mitochondrial dynamics such as *Opa1*, as well as of genes involved in
110 mitochondrial membrane and cristae organisation such as *Samm50* (Fig. 3c), suggesting that
111 mitochondrial function is impaired in loser cells.

112 A recent body of evidence has revealed that stress responses, such as the integrated stress
113 response (ISR) or the closely related unfolded protein response (UPR), when triggered in cells
114 with impaired mitochondrial function prompt a transcriptional program to restore cellular
115 homeostasis²⁷⁻²⁹. We observed that loser epiblast cells displayed a characteristic UPR-ISR
116 signature³⁰⁻³³ and key regulators of this response, such as *Atf4*, *Ddit3*, *Nrf2* and *Foxo3* were all
117 up-regulated in these cells (Extended Data Fig. 4a-d). Similarly, *Sesn2*, a target of p53 that
118 controls mTOR activity³⁴, was also up-regulated in loser cells (Extended Data Fig. 4d). These
119 findings support that loser epiblast cells present mitochondrial defects, leading to the activation
120 of a stress response in an attempt to restore cellular homeostasis³⁵.

121 To validate the significance of the observed mitochondrial defects, we did two things. First, we
122 asked if the changes of mitochondrial regulators at the mRNA level are also reflected at the
123 protein level. We observed that in CI-treated embryos, loser cells that persist and are marked by
124 low mTOR activity⁷, also show significantly lower OPA1 levels (Fig. 3d-f). We also found that
125 DMSO-treated embryos showed strong DDIT3 staining (an UPR-ISR marker) in the dying cells
126 that accumulate in the proamniotic cavity, and that in CI-treated embryos, DDIT3 expression was
127 up-regulated in a proportion of epiblast cells (Extended Data Fig. 4e-g). The second thing we did
128 to validate the importance of the mitochondrial defects was to study in loser epiblast cells their
129 mitochondrial membrane potential ($\Delta\psi_m$), an indication of mitochondrial health. We observed
130 that while the cells of DMSO-treated embryos showed a high $\Delta\psi_m$ that fell within a narrow
131 range, in CI-treated embryos the proportion of cells with a low $\Delta\psi_m$ significantly increased (Fig.
132 3d and 3g-h). Together, these results suggest that loser epiblast cells have impaired
133 mitochondrial activity that triggers a stress response.

134 **Mitochondrial dysfunction is common to different types of loser cells**

135 To address if mitochondrial defects are a common feature of loser cells eliminated by cell
136 competition, we analysed ESCs that are defective for BMP signalling (*Bmpr1a*^{-/-}) and tetraploid
137 cells (4n)⁶. We first carried out a mass spectrometry analysis using the Metabolon platform and
138 found that metabolites and intermediates of the TCA cycle, such as malate, fumarate, glutamate
139 and α -ketoglutarate are depleted in both *Bmpr1a*^{-/-} and 4n ESCs in differentiation culture
140 conditions (Fig. 4a). Next, we performed an extracellular flux Seahorse analysis of *Bmpr1a*^{-/-}
141 ESCs to measure their glycolytic and oxidative phosphorylation (OXPHOS) rates. We observed
142 that when these cells are maintained in pluripotency culture conditions that are not permissive
143 for cell competition⁶, they showed a similar glycolytic activity but a higher OXPHOS rate than
144 control cells (Extended Data Fig. 5a-b). In contrast, when *Bmpr1a*^{-/-} cells are induced to
145 differentiate, this phenotype is reversed, with mutant cells showing lower ATP generated through
146 OXPHOS and a higher glycolytic capacity than controls (Fig. 4b-e and Extended Data Fig. 5c-d).
147 This suggests that upon differentiation *Bmpr1a*^{-/-} cells are unable to sustain proper OXPHOS
148 activity.

149 To further test the possibility that defective ESCs have impaired mitochondrial function, we
150 assessed their $\Delta\psi_m$. We found that whilst *Bmpr1a*^{-/-} and 4n cells had a similar $\Delta\psi_m$ to control
151 cells in pluripotency conditions (Extended Data Fig. 5e-f), upon differentiation both these cell
152 types presented a loss of $\Delta\psi_m$, irrespective of whether they were separate or co-cultured with
153 wild-type cells (Fig. 4f-g). This reduction in $\Delta\psi_m$ is not due to excessive mitochondrial reactive
154 oxygen species (ROS) production or to a lower mitochondrial mass within mutant cells since, as
155 for example, *Bmpr1a*^{-/-} cells have lower ROS levels and similar TOMM20 and mt-CO1
156 expression as control cells (Fig. 4h-j and Extended Data Fig. 5g). The fact that the loss of $\Delta\psi_m$
157 and lower OXPHOS activity can be observed even when loser cells are cultured separately,
158 suggests that the mitochondrial dysfunction phenotype is an inherent property of loser cells and
159 not a response to them being out-competed. These results also indicate that the mitochondrial
160 defects are directly linked to the emergence of the loser status: in conditions that are not
161 permissive for cell competition (pluripotency) mutant cells do not show defective mitochondrial

162 function, but when they are switched to differentiation conditions that allow for cell competition,
163 they display impaired mitochondrial function.

164 To further explore the relationship between mitochondrial activity and the competitive ability of
165 the cell, we analysed the $\Delta\psi_m$ of BMP defective cells that are null for p53 (*Bmpr1a*^{-/-}; *p53*^{-/-}
166 ESCs), as these are not eliminated by wild-type cells⁷. Remarkably, we observed that mutating
167 *p53* in *Bmpr1a*^{-/-} cells not only rescues the loss of $\Delta\psi_m$ of these cells, but also causes
168 hyperpolarisation of their mitochondria (Fig. 4k). These results not only suggest a role for P53 in
169 regulating mitochondrial activity of ESCs, but also strongly support a pivotal role for
170 mitochondrial activity in cell competition.

171 **Impaired mitochondrial function is sufficient to trigger cell competition**

172 The mitochondrial defects observed in loser cells led us to ask if disrupting mitochondrial activity
173 alone is sufficient to trigger cell competition. During the onset of differentiation, mitochondrial
174 shape changes substantially. In pluripotent cells mitochondria have a round and fragmented
175 shape, but upon differentiation they fuse and become elongated, forming complex networks¹⁰.
176 Given that this change in shape correlates with when cell competition occurs, we tested if
177 disrupting mitochondrial dynamics is sufficient to induce cell competition. MFN1 and MFN2
178 regulate mitochondrial fusion and DRP1 controls their fission³⁶⁻³⁸. We generated *Mfn2*^{-/-} ESCs,
179 that have enlarged globular mitochondria, and *Drp1*^{-/-} ESCs, that show hyper-elongated
180 mitochondria (Fig. 5a). We observed that *Mfn2*^{-/-} ESCs displayed very poor growth upon
181 differentiation (data not shown). For this reason, we tested their competitive ability in
182 pluripotency conditions, that we have previously found not to induce the out-competition of
183 *Bmpr1a*^{-/-} or 4n cells⁶. Interestingly, we found that although *Mfn2*^{-/-} cells grow similarly to wild-
184 type cells in separate cultures, they were out-competed in co-culture (Fig. 5b). Analysis of the
185 *Drp1* mutant cells showed that although they did not grow significantly slower than wild-type
186 cells when cultured separately in differentiation inducing conditions, they were out-competed by
187 wild-type cells in co-culture (Fig. 5c). The observation that disrupting mitochondrial dynamics

188 can induce cell competition even in pluripotency culture conditions, suggests that mitochondrial
189 activity is a dominant parameter determining the competitive ability of the cell.

190 To establish how disruption of mitochondrial fusion and fission affects mitochondrial
191 performance we compared the $\Delta\psi_m$, respiration rates and mitochondrial ATP production of
192 *Mfn2*^{-/-} and *Drp1*^{-/-} ESCs to that of wild-type cells (Fig. 5d-g). We found that whilst *Mfn2*^{-/-} and
193 *Drp1*^{-/-} ESCs had lower $\Delta\psi_m$ than control cells (Fig. 5d,f), *Mfn2*^{-/-} ESCs had lower maximal
194 respiration rates but similar basal respiration and ATP production to controls and *Drp1*^{-/-} ESCs
195 showed similar respiration and ATP production to controls (Fig. 5e,g). This suggests that ATP
196 production or respiration rates alone do not determine the relative competitive ability of ESCs.

197 Besides mitochondrial dysfunction, another prominent signature of loser cells found *in vivo* was
198 the UPR/ISR (Ext. Data Fig. 4). Since the loss of *Drp1* has been associated with activation of the
199 UPR³⁹⁻⁴¹, we investigated if the *Drp1*^{-/-} loser cells also showed evidence for the activation of the
200 UPR/ISR. We observed that *Drp1*^{-/-} cells show higher expression of ATF4 and p-eIF2 α than wild-
201 type counterparts, which is indicative of UPR/ISR activation (Fig. 5h)³⁹⁻⁴¹. Another feature
202 previously described upon loss of *Drp1* is the proteolytic cleavage of OPA1, where short
203 isoforms (S-OPA1) are accumulated in detriment of the long isoforms (L-OPA1)³⁹. When we
204 analysed the expression of OPA1 in wild-type and *Drp1*^{-/-} cells we observed that while wild-type
205 cells retain L-OPA1 expression, loser cells predominantly express the S-OPA1 isoforms and
206 display almost no expression of L-OPA1 (Fig. 5i). This defect has been associated with mito-
207 ribosomal stalling, a phenotype that can be replicated by treating cells with actinonin (Extended
208 Data Fig. 6)⁴². To test if the shift in isoform expression observed in *Drp1*^{-/-} ESCs is due to
209 aberrant mitochondrial translation we treated cells with doxycycline, that inhibits this
210 translation⁴³, and observed that this was sufficient to partially rescue L-OPA1 expression (Fig.
211 5j). This rescue together with the evidence for UPR/ISR expression suggest that *Drp1*^{-/-} cells
212 display defects in mitochondrial translation.

213 **Loser epiblast cells accumulate mtDNA mutations**

214 There is strong evidence for selection against aberrant mitochondrial function induced by
215 deleterious mtDNA mutations in mammals^{21, 44-47}. Given that we observe that cell competition
216 selects against cells with impaired mitochondrial function, we asked if cell competition could be
217 reducing mtDNA heteroplasmy (frequency of different mtDNA variants) during mouse
218 development. It has been recently shown that scRNA-seq can be used to reliably identify mtDNA
219 variants, although with a lower statistical power compared to more direct approaches, like
220 mtDNA sequencing⁴⁸. We therefore tested if mtDNA heteroplasmy is present in our scRNA-seq
221 data and whether this correlates with the losing score of a cell. Our analysis revealed that the
222 frequency of specific mtDNA polymorphisms increased with the losing score of epiblast cells
223 (Fig. 6a), and such mtDNA changes occurred within *mt-Rnr1* and *mt-Rnr2* (Fig. 6b-h and
224 Extended Data Fig. 7a-e). Moreover, these changes were not dependent on the litter from which
225 the embryo came from (Extended Data Fig. 7f-k). The mutations we detected in *mt-Rnr1* and *mt-*
226 *Rnr2* strongly co-occurred in the same cell, with those closest together having the highest
227 probability of co-existing (Fig. 6i and Extended Data Fig. 7l). This is suggestive of mtDNA
228 replication errors that could be 'scarring' the mtDNA, disrupting the function of *mt-Rnr1* (12S
229 rRNA) and *mt-Rnr2* (16S rRNA) and causing the loser phenotype. Importantly, the presence of
230 these specific mtDNA mutations in the loser cells suggests that cell competition is contributing to
231 the elimination of deleterious mtDNA mutations during early mouse development.

232 **Changes in mtDNA sequence can determine the competitive ability of a cell**

233 To explore this possibility further, we analysed if alterations in mtDNA can induce cell
234 competition by testing the competitive ability of ESCs with non-pathological differences in
235 mtDNA sequence. For this we compared the relative competitive ability of ESCs that shared the
236 same nuclear genome background but differed in their mitochondrial genomes by a small
237 number of non-pathological sequence changes. We derived ESCs from hybrid mouse strains
238 that we had previously engineered to have a common nuclear C57BL/6N background, but
239 mtDNAs from different wild-caught mice¹⁶. Each wild-derived mtDNA variant (or haplotype)
240 contains a specific number of single nucleotide polymorphisms (SNPs) that lead to a small

241 number of amino acid changes when compared to the C57BL/6N mtDNA haplotype.
242 Furthermore, these haplotypes (BG, HB and ST) can be ranked according to their genetic
243 distance from the C57BL/6N mtDNA (Fig. 7a and Extended Data Fig. 8a). Characterization of
244 the isolated ESCs revealed that they have a range of heteroplasmy (mix of wild-derived and
245 C57BL/6N mtDNAs) that is stable over several passages (Extended Data Fig. 8b). Importantly,
246 these different mtDNA haplotypes and different levels of heteroplasmy do not alter cell size, cell
247 granularity, mitochondrial mass or mitochondrial dynamics, nor do they substantially impact the
248 cell's $\Delta\psi_m$ (Extended Data Fig. 8c-f).

249 When we tested the competitive ability of these ESCs with different mtDNA content, in
250 pluripotency culture conditions, we observed that cells carrying the mtDNAs that are most distant
251 from the C57BL/6N mtDNA, such as the HB(100%), the HB(24%) and the ST(46%) ESCs could
252 all out-compete the C57BL/6N line (Fig. 7b-c and Extended Data Fig. 8g). Similarly, when we
253 tested the HB(24%) line against the BG(99%) or the BG(95%) lines (that have mtDNAs more
254 closely related to the C57BL/6N mtDNA), we found that cells with the HB haplotype could also
255 out-compete these ESCs (Fig. 7d and Extended Data Fig. 8h). In contrast, we observed that the
256 HB(24%) ESCs were unable to out-compete either their homoplasmic counterparts, HB(100%),
257 or the ST(46%) cells that carry the most distant mtDNA variant from C57BL/6N (Fig. 7e and
258 Extended Data Fig. 8i). These results tell us three things. First, that non-pathological differences
259 in mtDNA sequence can trigger cell competition. Second, that a competitive advantage can be
260 conferred by only a small proportion of mtDNA content, as indicated by our finding that HB(24%)
261 behave as winners. Finally, these findings suggest that the phylogenetic proximity between
262 mtDNA variants can potentially determine their competitive cell fitness.

263 To characterise the mode of competition between cells with different mtDNA we focussed on the
264 HB(24%) and the BG(95%) ESCs. Analysis of these cell lines revealed that specifically when co-
265 cultured, the BG(95%) cells display high levels of apoptosis (Fig. 7f), indicating that their out-
266 competition is through their elimination. To gain further insight we performed bulk RNA-seq of
267 these cells in separate and co-culture conditions (Extended Data Fig. 8j) and analysed the

268 differentially expressed genes by gene-set enrichment analysis (GSEA). We found that in
269 separate culture the most notable features that distinguish BG(95%) from HB(24%) cells were a
270 down-regulation of genes involved in oxidative phosphorylation and an up-regulation of those
271 associated with cytokine activity (Fig. 8g). Interestingly, in the co-culture condition, in addition to
272 these signatures, BG(95%) cells revealed a down-regulation in signature markers of MYC
273 activity and mTOR signalling (Fig. 7h), whose downregulation are known read-outs of a loser
274 status during cell competition in the embryo⁵⁻⁷ (Fig. 2c).

275 To test if the down-regulation of genes involved in oxidative phosphorylation was also reflected
276 at the functional level we compared oxygen consumption rates and mitochondrial ATP
277 generation in HB(100%), HB(24%), BG(95%) and C57Bl/6N ESCs. We find that the winner cells
278 HB(100%) and HB(24%) have higher basal respiration, higher maximal respiration and higher
279 mitochondrial ATP production than the loser BG(95%) and C57BL/6N ESCs (Extended Data Fig.
280 9). These data indicate that the mtDNA differences that exist between winner and loser cells are
281 sufficient to affect their mitochondrial performance and this ultimately determines their
282 competitive ability. However, the observation that differentiating *Drp1*^{-/-} ESCs are eliminated by
283 cell competition but do not show differences in respiration rates or mitochondrial ATP production
284 (Fig. 5b,e), suggests that respiration or ATP production rates alone are unlikely to be the
285 mitochondrial parameters that control competitive cell fitness.

286 The finding that the genes down-regulated in BG(95%) cells when co-cultured with HB(24%)
287 cells fell under functional categories relating to mitochondrial function (Extended Data Fig. 10a)
288 led us to analyse the degree of overlap between these genes and the genes differentially
289 expressed along the winner-to-loser trajectory in the embryo. We observed a significant overlap
290 in mis-regulated genes (Extended Data Fig. 10b), as well as in the functional components that
291 these genes can be categorised into (Extended Data Fig. 10c). This further highlights the
292 importance of relative mitochondrial activity for determining the competitive ability of embryonic
293 cells.

294 **Discussion**

295 The emerging role of cell competition as a regulator of cell fitness in a wide range of cellular
296 contexts, from the developing embryo to the ageing tissue¹⁻³, has highlighted the importance of
297 understanding what cell types are normally eliminated by this process. With the aim of
298 understanding this question, we have analysed the transcriptional identity of the cells eliminated
299 in the early mouse embryo. We have found not only that they present a cell competition
300 signature but also that they are marked by mtDNA mutations and impaired mitochondrial
301 function. Starting from these results, we leveraged *in vitro* models of cell competition to show
302 that: (i) mitochondrial function is impaired in loser cells eliminated by cell competition, and (ii)
303 differences in mitochondrial activity are sufficient to trigger cell competition in ESCs. Overall, this
304 points to mitochondrial performance as a key determinant of the competitive ability of cells
305 during early mammalian embryonic development. One implication of our findings is that a range
306 of different types of defects, such as mis-patterning, karyotypic abnormalities or mtDNA
307 mutations, all lead to dysfunctional mitochondria at the onset of differentiation and that ultimately
308 it is their impaired mitochondrial function that triggers cell competition, inducing their elimination
309 (Fig. 8).

310 Embryos are exposed to different microenvironments *in vivo* and when cultured *ex-vivo*.
311 Similarly, ESCs also experience a different micro-environment to epiblast cells in the
312 embryo. These different micro-environments could potentially affect the selective pressure and
313 hence the transcriptional signature of loser cells. However, there are two reasons why we think
314 that the loser cell signatures we identify here are conserved across systems. First, the
315 transcriptional profile of our epiblast cells from cultured embryos is very similar to that of epiblast
316 cells from freshly isolated embryos (see Extended Data Figure 3e-g). Second, the loser
317 signature identified here is enriched for targets of P53 and depleted for mTOR and c-MYC
318 targets. Given that these are regulators of cell competition identified by us and others in the
319 embryo and in ESCs⁵⁻⁷, it suggests that the same pathways are inducing loser cell elimination in
320 *in vivo*, *ex-vivo* and in ESC models of cell competition.

321 It is well known that the successful development of the embryo can be influenced by the quality
322 of its mitochondrial pool¹⁰. Moreover, divergence from normal mitochondrial function during
323 embryogenesis is either lethal or can lead to the development of mitochondrial disorders⁴⁹.
324 Deleterious mtDNA mutations are a common cause of mitochondrial diseases and during
325 development selection against mutant mtDNA has been described to occur through at least two
326 mechanisms: the bottleneck effect and the intra-cellular purifying selection. The bottleneck effect
327 is associated specifically with the unequal segregation of mtDNAs during primordial germ cell
328 specification, for example as seen in the human embryo⁵⁰. In contrast to this, purifying selection,
329 as the name implies, allows for selection against deleterious mtDNAs and has been proposed to
330 take place both during development and post-natal life⁵¹. Importantly, purifying selection has
331 been found to occur at the molecule and organelle level, as well as at the cellular level⁵². Our
332 findings indicate that purifying selection can occur not only at the intra-cellular level but also
333 inter-cellularly (cell non-autonomously). We show that epiblast cells are able to sense their
334 relative mitochondrial activity and that those cells with mtDNA mutations, lower or aberrant
335 mitochondrial function are eliminated. By selecting those cells with the most favourable
336 mitochondrial performance, cell competition would not only prevent cells with mitochondrial
337 defects from contributing to the germline or future embryo, but also ensure optimisation of the
338 bioenergetic performance of the epiblast, therefore contributing to the synchronization of growth
339 during early development.

340 Cell competition has been studied in a variety of organisms, from *Drosophila* to mammals, and it
341 is likely that multiple different mechanisms fall under its broad umbrella¹⁻³. In spite of this, there
342 is considerable interest in understanding if there could be any common feature in at least some
343 of the contexts where cell competition has been described. The first demonstration of cell
344 competition in *Drosophila* was made by inducing clones carrying mutations in the ribosomal
345 gene *Minute*⁴ and this has become one of the primary models to study this process. Our finding
346 that during normal early mouse development cell competition eliminates cells carrying mutations
347 in *mt-Rnr1* and *mt-Rnr2*, demonstrates that in the physiological context mutations in ribosomal

348 genes also trigger cell competition. Furthermore, our observation that mis-patterned and
349 karyotypically abnormal cells show impaired mitochondrial activity indicates that during early
350 mouse development different types of defects impair mitochondrial function and trigger cell
351 competition. Interestingly, mtDNA genes are amongst the top mis-regulated factors identified
352 during cell competition in the mouse skin⁵³. In the *Drosophila* wing disc oxidative stress, a
353 general consequence of dysfunctional mitochondria, underlies the out-competition of *Minute* and
354 *Mah-jong* mutant cells⁵⁴. Similarly, in MDCK cells a loss of $\Delta\psi_m$ occurs during the out-
355 competition of RasV12 mutant cells and is key for their extrusion⁵⁵. These observations raise the
356 possibility that differences in mitochondrial activity may be a key determinant of competitive cell
357 fitness in a wide range of systems. Unravelling what mitochondrial features can lead to cellular
358 differences that can be sensed between cells during cell competition and if these are conserved
359 in human systems will be key not only for understanding this process, but also to open up the
360 possibility for future therapeutic avenues in the diagnosis or prevention of mitochondrial
361 diseases.

362 **Acknowledgments**

363 We would like to thank Stephen Rothery for guidance and advice with confocal microscopy. The
364 Facility for Imaging by Light Microscopy (FILM) at Imperial College London is part-supported by
365 funding from the Wellcome Trust (grant 104931/Z/14/Z) and BBSRC (grant BB/L015129/1). We
366 thank James Elliot and Bhavik Patel from the LMS/NIHR Imperial Biomedical Research
367 Centre Flow Cytometry Facility for support. We are thankful to George Chennell and Alessandro
368 Sardini for guidance and support with Seahorse experiments. We also want to acknowledge
369 Thomas Kolbe from University of Veterinary Medicine (Vienna) for isolating embryos from hybrid
370 mice strains from which mESCs were derived. Research in Tristan Rodriguez lab was supported
371 by the MRC project grant (MR/N009371/1) and by the British Heart Foundation centre for
372 research excellence. Work in the Scialdone lab is funded by the Helmholtz Association. Ana
373 Lima was funded by a BHF centre of excellence PhD studentship. Shankar Srinivas was funded
374 through Wellcome awards 103788/Z/14/Z and 108438/Z/15/Z.

375 **Author Contributions**

376 A.L. performed most of the experimental wet lab work. J.B. and A.L. derived heteroplasmic
377 mESC lines. J.B. performed heteroplasmy measurements in heteroplasmic mESCs. B.P.
378 generated *Mfn2*^{-/-} and *Drp1*^{-/-} mESCs and J.M.S did characterisation of mitochondria shape and
379 pluripotency status. S.P.M participated in the metabolic characterisation of *Drp1*^{-/-} cells. D.H.
380 performed embryo dissections, treatments and cell dissociation prior to scRNA-seq experiments.
381 G.L. did the bioinformatic analysis of scRNA-seq data. E.M., N.J. and A.G. participated in the
382 analysis of mitochondrial DNA heteroplasmy. A.D.G. performed the metabolomic studies using
383 Metabolon platform and participated in embryo dissections and immunohistochemistry stainings
384 for validation of results obtained by scRNA-seq. M.D, and M.K. performed the bioinformatic
385 analysis of bulk RNA-seq experiments. N.J., S.S. and D.C. participated in the design of
386 experimental work and analysis of results. A.L., G.L., A.S and T.R. interpreted results and wrote
387 the paper. T.R. and A.S. directed and designed the research.

388 **Competing Interests**

389 The authors declare no competing interests.

390 **Figure titles and legends**

391 **Fig. 1 | Cells eliminated during early mouse embryogenesis have a distinct transcriptional**
392 **profile.**

393 **a**, Experimental design. The number of cells in the two conditions (DMSO-treated and CI-
394 treated) refers to the number of cells that passed the quality control. **b**, Identification of the
395 clusters according to known gene markers from the different embryonic regions⁵⁶. Three clusters
396 (clusters 1, 3 and 4) show marker genes of the epiblast (Epi), while the remaining clusters
397 correspond to the extra-embryonic lineages visceral endoderm (VE; cluster 5) and
398 extraembryonic ectoderm (ExE; cluster 2). The epiblast clusters are named “Winner”,
399 “Intermediate” and “Loser” on the basis of the relative fraction of cells from CI-treated embryos
400 they include (see panel **e**). **c,d**, UMAP visualization of the single-cell RNA-seq data, with cells
401 coloured according to cluster (**c**) or condition (**d**). A region made up exclusively by cells from CI-
402 treated embryos emerges. **e**, Ratio between the fraction of cells from DMSO-treated and CI-
403 treated embryos in the three epiblast clusters. While the “winner” epiblast cluster shows an
404 enrichment of cells from DMSO-treated embryos, the “intermediate” and the “loser” epiblast
405 clusters are strongly enriched for cells from CI-treated embryos.

406 **Fig. 2 | A cell competition transcriptional signature is identified in cells eliminated during**
407 **mouse embryonic development.**

408 **a**, Diffusion map of epiblast cells (only from CI-treated embryos), coloured by cluster. **b, c**, IPA
409 run on the list of genes differentially expressed along the diffusion trajectory (see Extended Data
410 Fig. 2a) generated lists of top 5 molecular and cellular functions (**b**) and upstream regulators (**c**)
411 found to be differentially activated in epiblast cells along the diffusion trajectory from winner
412 (cluster 1) to loser status (cluster 4). **d**, Diffusion map of epiblast cells (only from CI-treated
413 embryos) coloured by diffusion pseudotime coordinate (dpt). The winner and the loser clusters
414 are found at the two extremities of the trajectory, hence the dpt can be interpreted as a “losing
415 score”. **e**, Losing score of the cells in the three epiblast clusters in CI-treated (left) or DMSO-
416 treated (right) embryos. The losing score of the cells from DMSO-treated embryos was obtained

417 by projecting them on the diffusion map shown in panel **d** (see Methods). **f**, Expression levels in
418 epiblast cells from CI-treated embryos of genes (in rows) that are markers for naïve pluripotency
419 (*Klf4*, *Klf5*, *Sox2*, *Pou3f1*, *Tcf7l1* and *Pou5f1* and *Rex1*), primed pluripotency (*Fgf5* and *TdGF1*),
420 mesoderm (*Mesp1* and *T*), neuroectoderm (*Neurod1* and *Sox1*) and endoderm (*Sox17* and
421 *Gata6*). Cells (in columns) are sorted by their losing scores. The genes marked with a * are
422 differentially expressed along the trajectory.

423 **Fig. 3 | Cells eliminated during early mouse embryogenesis have mitochondrial defects.**

424 **a**, Top canonical pathways, identified by IPA, mis-regulated in loser cells in comparison to
425 normal epiblast cells. The numbers at the end of each bar refer to total amount of genes
426 involved in that pathway. The percentage refers to the number of genes found mis-regulated in
427 loser cells relative to the number total genes within each pathway. Statistical significance
428 calculated with Fisher's exact test ($p < 0.05$): Mitochondrial Dysfunction, $-\log_{10}(p\text{-value}) = 21.1$;
429 Oxidative Phosphorylation, $-\log_{10}(p\text{-value}) = 18.6$; EIF2 signalling, $-\log_{10}(p\text{-value}) = 11.9$. **b**,
430 Detail of changes in oxidative phosphorylation pathway identified in (**a**). Circular and oval shapes
431 represent each of the ETC complexes (complexes I to V). Diamond shapes represent subunits
432 of each ETC complex. Genes that are down-regulated in loser cells are coloured in shades of
433 red. Darker shades correspond to lower values of FDR, which ranges from $1.25E-51$ (for *Atp5b*)
434 to $5.42E-03$ (for *Ndufa11*). *Cox6b2*, coloured in yellow, was found to be up-regulated in loser
435 cells ($FDR = 2.69E-13$). Grey colour denotes genes that were not differentially expressed
436 between loser and winner cells ($FDR > 0.01$). White colour denotes genes from the Knowledge
437 Base that were not tested (e.g., because they were not detected in our dataset). **c**, Expression
438 levels of some mitochondrial genes as a function of cells' losing score. *mt-Atp6*, mitochondrial
439 DNA encoded ATP synthase membrane subunit 6; *mt-Nd3*, mitochondrial DNA encoded NADH
440 dehydrogenase subunit 3; *Opa1*, optic atrophy 1; *Samm50*, sorting and assembly machinery
441 component 50 homolog. **d**, Experimental design adopted to assess mitochondria function (OPA1
442 expression, by immunofluorescence or $\Delta\psi_m$, given by TMRM fluorescence) in epiblast cells
443 from embryos where cell death was allowed (DMSO-treated) or inhibited (CI-treated). *

444 Micrograph of isolated epiblast (arrow) after embryo microdissection. **e**, Representative
445 immunohistochemistry of OPA1 in E6.5 embryo where cell death was inhibited (CI-treated),
446 quantified in **(f)**. Loser cells are identified by low mTOR activation (low p-rpS6, arrowheads).
447 Scale bar = 20 μ m. **f**, Quantification of OPA1 fluorescence in normal epiblast cells and loser
448 cells. N=6 embryos with a minimum of 8 cells analysed per condition. Statistical analysis
449 performed by Mann-Whitney test. **g**, Representative histogram of flow cytometry analysis of
450 TMRM probe, indicative of $\Delta\psi$ m, in epiblast cells from embryos where cell death was allowed
451 (DMSO-treated) or inhibited (CI-treated), quantified in **(h)**. **h**, Frequency of epiblast cells with
452 high or low TMRM fluorescence, according to range defined in **(g)** from embryos where cell
453 competition was allowed (DMSO treated) or inhibited (CI-treated). Statistical analysis done by
454 two-way ANOVA, followed by Holm-Sidak's multiple comparisons test. N=3 independent
455 experiments. Data shown as mean \pm SEM.

456 **Fig. 4 | Mitochondrial defects are a common feature of cells eliminated by cell**
457 **competition.**

458 **a**, Metabolic enrichment analysis of the TCA cycle and intermediate metabolites obtained using
459 Metabolon platform for defective cells (*Bmpr1a*^{-/-}, left bar and 4n, right bar), in comparison to
460 wild-type cells during differentiation. Bars indicate compound levels relative to wild-type cells.
461 Blue bars indicate compounds that are significantly depleted ($p < 0.05$) and light blue bars
462 indicate compounds that are almost significantly depleted ($0.05 \leq p \leq 0.1$). Black bars indicate
463 compounds that are depleted although not statistically significant in comparison to the levels
464 found in wild-type cells. The enzymes on the pathway are represented as boxes and labelled by
465 their canonical names. **b-e**, Metabolic flux analysis of wild-type and BMP-defective cells during
466 differentiating conditions. Data obtained with a minimum of 3 independent experiments, with 5
467 replicates per cell type in each assay. Statistical analysis done with Mann-Whitney test. Analysis
468 of oxygen consumption rate (OCR) as a measure of mitochondria function (mitochondria stress
469 test) **(b)**. Detail of metabolic parameters found changed from the analysis of the mitochondria
470 stress test **(c)**. Analysis of extracellular acidification rate (ECAR) as a measure of glycolytic

471 function (glycolysis stress test) (**d**). Detail of metabolic parameters found changed from the
472 analysis of the glycolysis stress test (**e**). **f-g**, Analysis of mitochondrial membrane potential
473 ($\Delta\psi_m$) in defective mESCs undergoing differentiation in separate or co-culture conditions.
474 Representative histograms of TMRM fluorescence and quantification for wild-type and *Bmpr1a*^{-/-}
475 (**f**) and wild-type and 4n (**g**). Statistical analysis done by two-way ANOVA, followed by Holm-
476 Sidak's multiple comparisons test. **h**, Representative micrographs of wild-type and *Bmpr1a*^{-/-}
477 cells co-cultured during differentiation and stained for a reporter of $\Delta\psi_m$ (MitoTracker Red, top
478 panel) or mitochondria mass (TOMM20, bottom panel). Nuclei are stained with Hoechst. Scale
479 bar = 10 μ m. **i-j**, Western blot analysis of mitochondria mass markers TOMM20 (**i**) and mt-CO1
480 (**j**) for wild-type and *Bmpr1a*^{-/-} cells during differentiation. Statistical analysis done with Mann-
481 Whitney test (**i**) or unpaired t-test (**j**). **k**, Analysis of mitochondrial membrane potential ($\Delta\psi_m$) for
482 wild-type, *Bmpr1a*^{-/-} and *Bmpr1a*^{-/-}; *p53*^{-/-} cells during differentiation. Representative histogram of
483 TMRM fluorescence and quantification. Statistical analysis done by one-way ANOVA, followed
484 by Holm-Sidak's multiple comparisons test. Data shown as mean \pm SEM of a minimum of 3
485 independent experiments.

486 **Fig. 5 | Manipulating mitochondria biology is sufficient to trigger cell competition.**

487 **a**, Representative micrographs of wild-type, *Mfn2*^{-/-} and *Drp1*^{-/-} mESCs showing alterations in
488 mitochondrial morphology in mutant cells. TOMM20 was used as a mitochondrial marker and
489 NANOG as a pluripotency marker. Nuclei are stained with Hoechst. Scale bar = 5 μ m. **b,c**, Cell
490 competition assays between wild-type mESCs and cells with altered morphology, *Mfn2*^{-/-} during
491 pluripotency (**b**) and *Drp1*^{-/-} during differentiation (**c**). The ratio of final/initial cell numbers in
492 separate or co-culture is shown. Statistical analysis done with two-way ANOVA, followed by
493 Holm-Sidak's multiple comparisons test. **d-j**, Metabolic profile of *Mfn2*^{-/-} and *Drp1*^{-/-} mESCs.
494 Analysis of mitochondrial membrane potential ($\Delta\psi_m$) for wild-type and *Mfn2*^{-/-} cultured
495 separately during pluripotency (**d**) and for wild-type and *Drp1*^{-/-} mESCs ^{-/-} after 3 days of
496 differentiation in separate culture (**f**). Data was obtained from 3 independent experiments and
497 statistical testing done with one sample t-test. Metabolic flux analysis of wild-type and *Mfn2*^{-/-}

498 mESCs cultured separately during pluripotency (e) and for wild-type and *Drp1*^{-/-} after 3 days of
499 differentiation in separate cultures (g). Data was collected from 3 independent experiments, with
500 5 replicates per cell type in each assay, and statistical testing done with Mann-Whitney test. h-j,
501 Western blot analysis of markers of UPR and mitochondrial markers in wild-type and *Drp1*^{-/-} after
502 3 days of differentiation in separate culture. Cells were treated with doxycycline (Dox, 22.5 μM)
503 or vehicle (Con) from day 1 of differentiation and samples were collected on day 3 (j). Statistical
504 analysis was done with an unpaired t-test (h-i) or two-way ANOVA followed by Holm-Sidak's
505 multiple comparisons test (j). Data shown as mean ± SEM of a minimum of 3 independent
506 experiments. p-eIF2α, phosphorylated eukaryotic initiation factor 2α.

507 **Fig. 6 | Intermediate and loser epiblast cells accumulate polymorphisms in mtDNA**
508 **sequence.**

509 a-g, mtDNA heteroplasmy in epiblast cells from CI-treated embryos. Average heteroplasmy
510 (considering all eleven polymorphisms that have a statistically significant dependence on the
511 losing score; see Methods) as a function of cells' losing scores. The p-value was computed with
512 a generalized linear model (a). mtDNA heteroplasmy for six positions within the *mt-Rnr1* gene
513 (b-g). The heteroplasmy at all of these positions as well as the average heteroplasmy increase
514 with the cells' losing scores in a statistically significant way (the adjusted p-value estimated via a
515 generalized linear model is indicated at the top of each plot). h, The barplot indicates the fraction
516 of epiblast cells in each of the cluster indicated on the x-axis (winner, intermediate, loser) that
517 carry a mean heteroplasmy (computed on the six positions within the *mt-Rnr1* indicated in the
518 panels b-g) greater than 0.01. This shows that the level of mtDNA heteroplasmy in *mt-Rnr1* is
519 strongly associated with the loser status of the cells, since ~55% and ~87% of cells in the
520 intermediate and the loser clusters, respectively, have heteroplasmic sequences in this gene
521 compared to only ~5% of cells in the winner cluster. i, Spearman's correlation coefficient
522 between the mtDNA heteroplasmy at the six positions shown in panels (b-g).

523 **Fig. 7 | Changes in mtDNA sequence can determine the competitive ability of a cell.**

524 **a**, Derivation of mESCs from hybrid mouse strains, generated elsewhere by Burgstaller and
525 colleagues. Neighbour-Joining Phylogenetic Analysis of mtDNA from wild and C57BL/6N mouse
526 strains, that were used to generate hybrid mice (adapted from¹⁶), illustrates the genetic distance
527 of the mtDNA from wild mouse strains to the C57BL/6N lab mouse. The number of single
528 nucleotide polymorphisms and amino acid changes (SNPs/ a.a. changes) from wild to lab mouse
529 strain is shown. mESCs were derived from embryos of hybrid mice, containing the nuclear
530 background of a C57BL/6N lab mouse and mtDNA from three possible wild-derived strains (BG,
531 HB or ST). **b-e**, Cell competition assays between cells derived from the embryos of hybrid mice
532 performed in pluripotency maintenance conditions. The ratio of final/initial cell numbers in
533 separate or co-culture is shown. Statistical analysis done with two-way ANOVA, followed by
534 Holm-Sidak's multiple comparisons test. **f**, Representative micrographs of cleaved caspase-3
535 staining and quantification of the percentage of apoptotic events in winners HB(24%) and loser
536 BG(95%) mESCs maintained pluripotent and cultured in separate or co-culture conditions.
537 Statistical analysis done with two-way ANOVA, followed by Holm-Sidak's multiple comparisons
538 test. **g-h**, Gene set enrichment analysis of differentially expressed genes from bulk RNA seq. in
539 loser BG (95%) compared to winner HB (24%) mESCs maintained pluripotent and cultured in
540 separate (**g**) or co-culture conditions (**h**). Gene sets that show positive normalized enrichment
541 scores (NES) are enriched in loser cells, while gene sets that show negative NES are depleted
542 in loser cells. Data in panels (**b-f**) shown as mean \pm SEM of a minimum of 3 independent
543 experiments.

544 **Fig. 8 | Model of cell competition.**

545 Summary of the main findings of the study. A range of cellular defects, such as aneuploidy, mis-
546 patterning or mtDNA mutations cause alterations in mitochondria function, which affect the
547 relative fitness of cells. The cells with suboptimal mitochondrial activity survive in a
548 homogeneous population but are eliminated by cell competition in the presence of fitter cells.

549 **Extended Data Fig. 1 | Quality controls of scRNA-seq and clustering robustness analysis.**

550 **a**, Selection criteria for quality control (QC) of all cells. A total of 723 passed the quality control
551 (723 good quality cells) and were considered for downstream analysis. All these parameters
552 were computed for each cell. Log₁₀ total number of reads (top left): log₁₀ of the sum of the
553 number of reads that were processed in every cell; Fraction of mapped reads (top central):
554 number of reads that are confidentially mapped to the reference genome divided by total number
555 of reads that were processed for each cell. This number is automatically provided by Salmon
556 v0.8.2; Fraction of genes (top right): number of reads mapped to endogenous genes divided by
557 the total sum of reads that were processed; Fraction of mt-genes (bottom left): number of reads
558 mapped to mitochondrial genes divided by the total sum of reads that were processed; Fraction
559 of spikes (bottom central): number of reads mapped to ERCC spike-ins divided by the total sum
560 of reads that were processed; Number of genes above 10 RPM (bottom right): number of genes
561 with expression level above 10 reads per million. **b**, Number of good quality cells in each
562 condition (rows) and batch (columns). **c**, Number of good quality cells per cluster (rows) and
563 batch (columns). **d**, UMAP plot of the data with cells coloured by batch. In each batch there is a
564 balanced distribution of cells in the two conditions and across the five clusters. **e**, The Pearson's
565 gamma (left panel) and the Average Silhouette Width (right panel) was calculated for each set of
566 clusters obtained with 100 random subsamples of 60% of highly variable genes and different
567 values of the deepSplit parameter (see Methods). The most robust clusters correspond to
568 deepSplit values of 0 and 1. **f**, The changes in composition and number of clusters between the
569 clustering obtained with deepSplit 0 (top) and 1 (bottom) are shown using the library "clustree"⁵⁷.

570 **Extended Data Fig. 2 | Cell cycle analysis and cluster connectivity.**

571 **a**, Cell cycle analysis of epiblast cells from clusters 1, 3 and 4. Cell cycle phase was predicted
572 with cyclone algorithm⁵⁸ and shows that there are cells in S and G2M phase also in the loser and
573 intermediate clusters. **b**, PAGA plot showing the connectivity of the five clusters of cells from CI-
574 treated embryos. **c-d**, Diffusion map analysis in all epiblast cells (from DMSO and CI-treated
575 embryos): cells are coloured according to the condition (**c**) and to the cluster (**d**). **e**, The pseudo-
576 time coordinate of the CI-treated epiblast cells obtained from the diffusion map including all

577 epiblast cells correlates extremely well with the pseudo-time coordinate obtained in the diffusion
578 map calculated only from CI-treated epiblast cells (Fig. 2a).

579 **Extended Data Fig. 3 | Analysis on epiblast cells from DMSO and CI-treated embryo.**

580 **a**, Heatmap showing the expression pattern of all genes differentially expressed along the
581 trajectory from winning to losing cells in Fig. 2d. **b-c**, Overlap of genes differentially expressed
582 along the trajectory joining winning and losing epiblast cells in CI-treated embryos (Fig. 2a and
583 panel d) and genes targeted by p53. Pie charts show the percentage of genes up- or down-
584 regulated in loser cells within the group of target genes that are activated (**b**) or repressed (**c**) by
585 p53. There is an enrichment of activated/repressed targets among genes
586 upregulated/downregulated in losing cells respectively (Fisher's test, p-value=1E-4). The list of
587 p53 targets is taken from⁵⁹. **d**, Scatter plots of the expression levels of different marker genes
588 plotted against each other in loser epiblast cells (cluster 4). Loser cells have higher expression
589 of pluripotency markers as well as higher expression of some lineage-specific markers and the
590 co-expression of these markers is only weakly correlated. **e-g** Our scRNA-seq data from epiblast
591 cells is projected on top of previously published data from epiblast collected from freshly isolated
592 embryos at different stages (E5.5, E6.25 and E6.5; data from²⁶). First, a diffusion map (**e**) and a
593 pseudotime coordinate (**f**) is computed for the epiblast cells from freshly isolated embryos. Then,
594 a pseudotime coordinate is estimated for our data after projecting it onto the diffusion map.
595 Panel **g** shows the pseudotime coordinates for both datasets, split by stage, treatment and
596 cluster.

597 **Extended Data Fig. 4 | Cells eliminated during early mouse embryogenesis have activated**
598 **stress responses.**

599 **a**, Overlap of genes differentially expressed along the trajectory joining winning and losing
600 epiblast cells in CI-treated embryos (Fig. 2a and Extended Data Fig. 3a) and genes related to
601 the unfolded protein response and integrated protein response pathways (UPR_ISR, see
602 Supplementary Table 3). From the 32 genes related to the UPR & ISR pathways, 12 are down-
603 regulated in loser cells, 8 genes are up-regulated in loser cells, and 12 genes are not

604 differentially expressed between loser and winner cells. There is a statistically significant
605 enrichment of UPR&ISR genes among the up-regulated genes in loser cells (Fisher test, odds
606 ratio=3.0, p-value=0.012). The intersection between UPR-ISR genes and the down regulated
607 genes is not significant (Fisher test, odds ratio=1.2, p value=0.69). **b-c**, List of genes from UPR-
608 ISR pathways that are statistically significantly up-regulated (**b**) or down-regulated (**c**) in loser
609 cells. **d**, Scatterplots with the expression levels of genes involved in stress responses in epiblast
610 cells from CI-treated embryos as a function of cells' losing score. **e**, Experimental design with the
611 approach taken to validate the expression of the stress response marker DDIT3 in epiblast cells
612 from DMSO or CI-treated embryos. **f**, Representative micrographs of DMSO (upper panel) or CI-
613 treated embryos (100 μ M, lower panel) stained for DDIT3, quantified in (**g**). Nuclei are labelled
614 with Hoechst. In control embryos (DMSO-treated), dying cells in the cavity show very high
615 DDIT3 expression (arrow), while live cells in the epiblast of the CI-treated embryos show more
616 modest levels of DDIT3 expression (arrowheads). Scale bar = 20 μ m. **g**, Quantification of the
617 percentage of epiblast cells with nuclear DDIT3 expression. N=10 DMSO and N=9 CI-treated
618 embryos. Data shown as mean \pm SEM. *Ddit3* (*Chop*), DNA-damage inducible transcript 3; *Atf3*,
619 activating transcription factor 3; *Atf4*, activating transcription factor 4; *Foxo3*, forkhead box O3;
620 *Ppp1r115a* (*Gadd34*), Protein Phosphatase 1 Regulatory Subunit 15A, *Eif2ak3* (*Perk*),
621 Eukaryotic Translation Initiation Factor 2 Alpha Kinase 3; *Nfe2l2* (*Nrf2*), NFE2-related factor 2;
622 *Sesn2*, Sestrin 2; *Gdf15*, Growth Differentiation Factor 15; *Mthfd1l*, Methylenetetrahydrofolate
623 Dehydrogenase (NADP⁺ Dependent) 1 Like; *Hspe1*, Heat Shock Protein Family E (*Hsp10*)
624 Member 1; *Cat*, Catalase; *Hspd1*, Heat Shock Protein Family D (Hsp60) Member 1; *Sod2*,
625 Superoxide Dismutase 2; *Hsph1*, Heat Shock Protein Family H (*Hsp110*) Member 1; *Lonp1*, Lon
626 Peptidase 1, Mitochondrial; *Eif2a*, Eukaryotic Translation Initiation Factor 2A; *Mthfd2*,
627 Methylenetetrahydrofolate Dehydrogenase (NADP⁺ Dependent) 2, Methenyltetrahydrofolate
628 Cyclohydrolase; *Hspa4*, Heat Shock Protein Family A (*Hsp70*) Member 4; *Cth*, Cystathionine
629 Gamma-Lyase; *Nrf1*, Nuclear Factor 1.

630 **Extended Data Fig. 5 | Mitochondrial function in Wild-type, *Bmpr1a*^{-/-} and 4n mESCs.**

631 **a-d**, Metabolic flux analysis of wild-type and *Bmpr1a*^{-/-} mESCs. OCR profile and metabolic
632 parameters assessed during the mitochondria stress test performed in pluripotency conditions
633 (a). ECAR profile and metabolic parameters assessed during the glycolysis stress test
634 performed in pluripotency conditions (b). Metabolic parameters from the mitochondria stress test
635 found to be similar between wild-type and *Bmpr1a*^{-/-} mESCs during differentiation – day 3 (c).
636 Metabolic parameters from the glycolysis stress test found to be similar between wild-type and
637 *Bmpr1a*^{-/-} mESCs during differentiation – day 3 (d). Data obtained with a minimum of 3
638 independent experiments, with 5 replicates per cell type in each assay. Statistical analysis done
639 with Mann-Whitney test. **e-f**, Analysis of mitochondrial membrane potential ($\Delta\psi_m$) in defective
640 mESCs maintained in pluripotency conditions, in separate or co-culture. Representative
641 histograms of TMRM fluorescence and quantification for wild-type and *Bmpr1a*^{-/-} (e) and wild-
642 type and 4n (f). Statistical analysis done by two-way ANOVA, followed by Holm-Sidak's multiple
643 comparisons test. **g**, Analysis of mitochondrial ROS in wild-type and *Bmpr1a*^{-/-} mESCs
644 undergoing differentiation in separate or co-culture: representative histograms of mitoSOX Red
645 fluorescence and quantification of the percentage of mitoSOX positive cells. Statistical analysis
646 done by two-way ANOVA, followed by Holm-Sidak's multiple comparisons test. Data obtained
647 with a minimum of 3 independent experiments. Error bars represent SEM.

648 **Extended Data Fig. 6 | Effect of actinonin in OPA1 expression in wild-type and *Drp1*^{-/-}**
649 **cells.** a, Western blot analysis of OPA1 expression in wild-type and *Drp1*^{-/-} cells treated with
650 actinonin (Act, 150 μ M) during 6 hours on the third day of differentiation, quantified in (b-c). **b-c**,
651 Expression levels of L-OPA1 (b) and S-OPA1 (c) relative to α -tubulin. Data shown as mean \pm
652 SEM of a minimum of 3 independent experiments. Statistical analysis done by two-way ANOVA,
653 followed by Holm-Sidak's multiple comparisons test.

654 **Extended Data Fig. 7 | Analysis of SNPs in mtDNA in epiblast cells.**

655 **a-e**, mtDNA heteroplasmy in epiblast cells from CI-treated embryos for five positions within the
656 *mt-Rnr2* gene. All of these positions have an heteroplasmy that increases with the cells' losing
657 scores in a statistically significant way (the adjusted p-value estimated via a generalized linear

658 model is indicated at the top of each plot). **f-k**, The variation in the heteroplasmy across the CI-
659 treated cells is not due to a batch effect for the 6 significant positions within the *mt-Rnr1* gene. **l**,
660 Spearman's correlation between the mtDNA heteroplasmy at all the statistically significant
661 positions (six within the gene *mt-Rnr1* and five within the gene *mt-Rnr2*).

662 **Extended Data Fig. 8 | Changes in mtDNA sequence are enough to trigger cell**
663 **competition.**

664 **a**, Illustration of the process of derivation of the mESCs lines from mice that are hybrid between
665 the wild-caught strains (BG, HB or ST) and the lab mouse (C57BL/6N). These hybrid mice were
666 generated elsewhere¹⁶ by ooplasmic transfer: the zygote of a C57BL/6N mouse was injected
667 with ooplasm from a wild-caught mouse (orange, HB pictured). Therefore, these hybrid mice
668 contain the nuclear background of the C57BL/6N strain and the mtDNA of wild-caught strain and
669 potentially C57BL/6N mtDNA (heteroplasmic mice strains). mESCs lines were derived from the
670 hybrid mice and characterised. **b-f**, Characterisation of the derived cell lines by flow cytometry,
671 during pluripotency, in comparison to the wild-type cell line used in previous experiments (E14,
672 129/Ola background). Heteroplasmy analysis of the derived mESC lines from the hybrid mice,
673 indicating the percentage of wild-derived mtDNA (**b**). Cell granularity (internal complexity) given
674 as median fluorescence intensity of SSc-A laser (**c**). Cell size given as median fluorescence
675 intensity of FSc-A laser (**d**). Analysis of the expression of mitochondrial markers: representative
676 western blot and quantification of markers of mitochondrial mass (ATPB, mt-CO1 and TOMM20)
677 and mitochondrial dynamics (DRP1, MFN1 and MFN2), relative to vinculin, in cells derived from
678 hybrid mice (**e**). **f**, Representative histograms and quantification of median TMRM fluorescence,
679 indicative of $\Delta\psi_m$, for the hybrid cell lines derived, in comparison to the wild-type cell line used in
680 previous experiments (E14, 129/Ola background). Statistical analysis done by one-way ANOVA,
681 followed by Holm-Sidak's multiple comparisons test. **g-i**, Cell competition assays between hybrid
682 cell lines maintained in pluripotency culture conditions. The ratio of final/initial cell numbers in
683 separate or co-culture is shown. Statistical analysis done by two-way ANOVA, followed by Holm-
684 Sidak's multiple comparisons test. **j**, Experimental design for RNA-Seq and gene set enrichment

685 analysis (GSEA). The isolation of RNA from winner HB(24%) and loser BG(95%) cells was
686 performed after three days in separate or co-culture conditions, once cells have been subjected
687 to FACS to isolate the two populations from mixed cultures. Data obtained with a minimum of 3
688 independent experiments. Error bars represent SEM.

689 **Extended Data Fig. 9 | Metabolic flux analysis of the cells with different mtDNA variants:**
690 **HB(100%), HB(24%), BG(95%) and C57BL/6N.** **a**, OCR profile during mitochondria stress test
691 performed in pluripotency maintenance conditions. **b-i**, Metabolic parameters assessed during
692 the during the mitochondria stress test performed in pluripotency conditions. Data obtained with
693 a minimum of 3 independent experiments, with 5 replicates per cell type in each assay. Error
694 bars represent SEM. Statistical analysis done with Kruskal-Wallis test, followed by Dunn's
695 multiple comparison test.

696 **Extended Data Fig. 10 | Common features of scRNA-seq and bulk RNA-seq datasets.**
697 **a**, Terms significantly enriched among genes downregulated in BG(95%) (loser) ESCs *in vitro*
698 when co-cultured with HB(24%) cells. The loss of mitochondrial activity emerges as a common
699 feature between loser cells *in vivo* and *in vitro*. The gene enrichment analysis was performed
700 using g-profiler tool (see Methods). **b**, Intersection between differentially expressed genes along
701 the trajectory from winning to losing epiblast cells ("in_vivo_scRNA-seq"; Fig. 2a and Extended
702 Data Fig. 3a and genes differentially expressed between co-cultured HB(24%) (winner) and
703 BG(95%) (loser) ESCs ("in_vitro_bulk_RNA-seq"). "Up" and "Down" here refer to genes up- or
704 down-regulated in loser cells. Fisher test for the intersection between down-regulated genes
705 from scRNA-seq (*in vivo*) and down-regulated genes from bulk RNA-seq (*in vitro*): p-value,
706 1.71E-12; odds ratio 1.80. Fisher test for the intersection between down-regulated genes from
707 scRNA-seq (*in vivo*) and up-regulated genes from bulk RNA-seq (*in vitro*): p-value, 5.20E-3;
708 odds ratio 0.67. Fisher test for the intersection between up-regulated genes from scRNA-seq (*in*
709 *vivo*) and down-regulated genes from bulk RNA-seq (*in vitro*): Fisher test p-value, 4.87E-3; odds
710 ratio 0.80. The intersection between up-regulated genes from sc-RNA-seq (*in vivo*) and up-
711 regulated genes from bulk RNA-Seq (*in vitro*) is not statistically significant: Fisher test p-value:

712 0.30, odds ratio 1.14. **c**, Intersection between the significantly enriched terms in genes
713 upregulated or downregulated in loser cells in the epiblast of CI-treated embryos
714 (“*in_vivo*_scRNA-Seq”) or in our *in vitro* model of competition between co-cultured HB(24%)
715 (winner) and BG(95%) (loser) ESCs (“*in_vitro*_bulk_RNA-seq”). All the terms enriched among
716 downregulated genes *in vitro* are also enriched *in vivo*.

717 **List of Tables.**

718 **Supplementary Table 1.** List of genes down-regulated along the winner-to-loser trajectory in the
719 embryo.

720 **Supplementary Table 2.** List of genes up-regulated along the winner-to-loser trajectory in the
721 embryo.

722 **Supplementary Table 3.** Genes related to the unfolded protein response and integrated protein
723 response pathways (UPR_ISR) that were analysed in the genes differentially expressed along
724 the winner-to-loser trajectory.

725 **Supplementary Table 4.** List of background genes for the winner-to-loser trajectory in the
726 embryo.

727 **Supplementary Table 5.** List of genes down-regulated in BG(95%) cells when co-cultured with
728 HB(24%) cells.

729 **Supplementary Table 6.** List of genes up-regulated in BG(95%) cells when co-cultured with
730 HB(24%) cells.

731 **Supplementary Table 7.** List of background genes used for the analysis of genes differentially
732 expressed between co-cultured BG(95%) and HB(24%) cells.

733 **Methods**

734 **Animals**

735 Mice were maintained and treated in accordance with the Home Office's Animals (Scientific
736 Procedures) Act 1986 and covered by the Home Office project license PBBEBDCDA. All mice
737 were housed on a 10 hr-14 hr light-dark cycle with access to water and food *ad libitum*. Matings
738 were generally set up in the afternoon. Noon of the day of finding a vaginal plug was designated
739 embryonic day 0.5 (E0.5). Embryo dissection was performed at appropriate timepoints in M2
740 media (Sigma), using Dumont No.5 forceps (11251-10, FST). No distinction was made between
741 male and female embryos during the analysis.

742 **Cell lines, cell culture routine and drug treatments**

743 E14, kindly provided by Prof A. Smith, from Cambridge University, were used as wild-type
744 control cells tdTomato-labelled or unlabelled. GFP-labelled or unlabelled cells defective for BMP
745 signalling (*Bmpr1a*^{-/-}), tetraploid cells (4n) and *Bmp1a*^{-/-} null for p53 (*Bmpr1a*^{-/-};*p53*^{-/-}) are
746 described elsewhere^{6,7}. Cells null for Dynamin-related protein 1 (*Drp1*^{-/-}) or Mitofusin 2 (*Mfn2*^{-/-})
747 were generated by CRISPR mutagenesis. Cells with different mitochondrial DNA (mtDNA)
748 content in the same nuclear background were derived from embryos of hybrid mice, generated
749 elsewhere¹⁶.

750 Cells were maintained pluripotent and cultured at 37°C in 5% CO₂ in 25 cm² flasks (Nunc)
751 coated with 0.1% gelatin (Sigma) in DPBS. Growth media (ES media) consisted of GMEM
752 supplemented with 10% FCS, 1 mM sodium pyruvate, 2 mM L-glutamine, 1X minimum essential
753 media non-essential amino-acids, 0.1 mM β-mercaptoethanol (all from Gibco) and 0.1%
754 leukemia inhibitory factor (LIF, produced and tested in the lab). Cells derived from hybrid mice
755 (C57BL/6N nuclear background) were maintained on 0.2% LIF. The growth media was changed
756 daily, and cells were split every 3 days.

757 To manipulate mitochondrial translation during differentiation, wild-type and *Drp1*^{-/-} mESCs were
758 treated with doxycycline (Dox, 22.5 μM), from day 1 to day 3 of culture, or with actinonin (Act,

759 150 μ M), for 6 hours on day 3 of culture in N2B27 media (see Differentiation and Cell
760 competition assays). As control condition, cells were treated with vehicle (Con). Samples were
761 collected on day 3 of differentiation for western blot analysis.

762

763 **CRISPR mutagenesis**

764 Drp1 and Mfn2 knockout ESCs were generated by CRISPR-Cas9 mediated deletion of Drp1
765 exon 2 and Mfn2 exon 3 respectively. sgRNA guides flanking Drp1 exon 2 or Mfn2 exon 3 were
766 cloned into the PX459 vector (Addgene)⁶⁰: Drp1 exon 2 upstream sgRNA:
767 5' TGGAACGGTCACAGCTGCAC 3'; Drp1 exon 2 downstream sgRNA:
768 5' TGGTCGCTGAGTTTGAGGCC 3'; Mfn2 upstream sgRNA: 5' GTGGTATGACCAATCCCAGA
769 3'; Mfn2 downstream sgRNA: 5' GGCCGGCCACTCTGCACCTT 3'. E14 ESCs were co-
770 transfected with 1 μ g of each sgRNA expression using Lipofectamine 2000 (Invitrogen) according
771 to manufacturer's instructions. As control E14 ESCs were transfected in parallel with equal
772 amount of empty PX459 plasmid. Following 6 days of Puromycin selection, single colonies were
773 picked from both Drp1 sgRNA and empty vector transfected ESCs and screened for
774 mutations. Drp1 exon 2 deletion was confirmed by PCR genotyping using the following primers:
775 Drp1_genot F: 5' GGATACCCCAAGATTTCTGGA 3'; Drp1_genot R: 5'
776 AGTCAGGTAATCGGGAGGAAA 3', followed by Sanger Sequencing. Mfn2 exon 3 deletion was
777 confirmed by PCR genotyping using the following primers: Mfn2_genot F: 5'
778 CAGCCCAGACATTGTTGCTTA 3'; Mfn2_genot R: 5' AGCTGCCTCTCAGGAAATGAG 3',
779 followed by Sanger Sequencing.

780 **Derivation of mESCs from hybrid mouse strains and heteroplasmy determination**

781 The derivation of new mESC lines was adapted from⁶¹. Cells were derived from embryos of
782 hybrid mouse strains BG, HB and ST. These contain the mtDNA of C57BL/6N (B16) lab mouse
783 and mtDNA variants from wild-caught mice¹⁶.

784 Embryos were isolated at E2.5 (morula stage) and cultured in 4-well plates (Nunc, Thermo
785 Scientific) containing KSOM media (Millipore) plus two inhibitors (KSOM+2i): 1 μ M MEK inhibitor
786 PDO325901 (Sigma-Aldrich) and 3 μ M GSK-3 inhibitor CHIR9902 (Cayman Chemicals) for 2
787 days at 37°C in 5% CO₂ incubator. To reduce evaporation, the area surrounding the wells was
788 filled with DPBS. Embryos were further cultured in a fresh 4-well plates containing,
789 N2B27+2i+LIF media: N2B27 media supplemented with 1 μ M MEK inhibitor PDO325901 and 3
790 μ M GSK-3 inhibitor and 0.1% LIF for up to 3 days until reaching the blastocyst stage. Each
791 embryo was then transferred to a well of a 96-well plate coated with 0.1% gelatin in DPBS and
792 containing 150 μ L of N2B27+2i+LIF media per well. In these conditions, the embryos should
793 attach to the wells allowing the epiblast to form an outgrowth. This plate was then incubated at
794 37°C in 5% CO₂ incubator for 3 to 7 days until ES-like colonies start to develop from the epiblast
795 outgrowth. Cells were passaged by dissociation with Accutase (Sigma) and seeded in gradual
796 increasing surface area of growth (48-well, 24-well, 12-well plate, T12.5 and T25 flask), until new
797 cell lines were established. At this stage cells were weaned from N2B27+2i+LIF media and then
798 routinely cultured in ES media.
799 These new cell lines were then subjected to characterisation by flow cytometry (cell size,
800 granularity and mitochondrial membrane potential) and ARMS-qPCR assay¹⁶ (to determine
801 heteroplasmy).

802 **Embryo experiments**

803 Early mouse embryos were isolated at E5.5 (from pregnant CD1 females, purchased from
804 Charles River, UK). Following dissection from the decidua, embryos were cultured overnight in
805 N2B27 "poor" media (same formulation as N2B27 media but supplemented with 0.5xB27
806 supplement and 0.5xN2 supplement) with pan-caspase inhibitors (100 μ M, Z-VAD-FMK,
807 FMK001, R&D Systems, USA) or equal volume of vehicle (DMSO) as control. On the next
808 morning, embryos were processed for single cell RNA-Seq (scRNA-seq) or functional validation
809 ($\Delta\psi$ m analysis and immunohistochemistry for markers of loser cells).

810 For the scRNA-seq and $\Delta\psi$ m analysis embryos were dissociated into single-cells. Briefly, up to
811 12 embryos were dissociated in 600 μ L Accutase (A6964, Sigma, UK) during 12 min at 37°C,
812 tapping the tube every two minutes. Accutase was then neutralised with equal volume of FCS,
813 cells spun down and stained with TMRM, for $\Delta\psi$ m analysis, or directly re-suspended in 300 μ L
814 DPBS with 1% FCS, for single cell sorting and RNA-seq. Sytox blue (1:1000, S34857,
815 ThermoFisher Scientific, UK), was used as viability staining.

816 **Differentiation and Cell competition assays**

817 Cell competition assays between wild-type and *Bmpr1a*^{-/-}, 4n or *Drp1*^{-/-} cells were performed in
818 differentiating conditions. Cells were seeded onto fibronectin-coated plates (1:100, Merck) in
819 DPBS during 1h at 37°C and grown in N2B27 media - to promote the differentiation of mESCs
820 into a stage resembling the post-implantation epiblast, as cell competition was previously shown
821 to occur in these conditions⁶. N2B27 media consisted of 1:1 Dulbecco's modified eagle medium
822 nutrient mixture (DMEM/F12) and Neurobasal supplemented with N2 (1x) and B27 (1x)
823 supplements, 2 mM L-glutamine and 0.1 mM β -mercaptoethanol - all from Gibco. Cell
824 competition assays between wild-type and *Mfn2*^{-/-} and between mESCs with different mtDNA
825 content were performed in pluripotency maintenance conditions (ES media).

826 Cells were seeded either separately or mixed for co-cultures at a 50:50 ratio, onto 12 well plates,
827 at a density of 8E04 cells per well, except for assays between wild-type and *Mfn2*^{-/-} mESCs,
828 where 3.2E05 cells were seeded per well. The growth of cells was followed daily and compared
829 between separate or co-culture, to control for cell intrinsic growth differences, until the fourth day
830 of culture. Viable cells were counted daily using Vi-CELL XR Analyser (Beckman Coulter, USA),
831 and proportions of each cell type in co-cultures were determined using LSR II Flow Cytometer
832 (BD Bioscience), based on the fluorescent tag of the ubiquitously expressed GFP or TdTomato
833 in one of the cell populations.

834 **Metabolomic analysis**

835 The metabolic profile was obtained using the Metabolon Platform (Metabolon, Inc). Each sample
836 consisted of 5 biological replicates. For each replicate, 1E07 cells were spun down and snap
837 frozen in liquid nitrogen. Pellets from 5 independent experiments for each condition were
838 analysed by Metabolon Inc by a combination of Ultrahigh Performance Liquid Chromatography-
839 Tandem Mass Spectroscopy (UPLC- MS/MS) and Gas Chromatography-Mass Spectroscopy
840 (GC-MS). Compounds were identified by comparison to library entries of purified standards
841 based on the retention time/index (RI), mass to charge ratio (m/z), and chromatographic data
842 (including MS/MS spectral data) on all molecules present in the library. Samples were
843 normalized to protein content measured by Bradford assay. Statistical analysis was done using
844 Welch's two-sample t-test and statistical significance defined as $p \leq 0.05$.

845 **Seahorse analysis**

846 The metabolic function of cells was assessed by extracellular flux analysis using Seahorse XF24
847 (Agilent Technologies, UK). For assays ran during pluripotency, cells were seeded, on the day
848 prior to the assay, onto 0.1% gelatin-coated (Sigma, UK) in 300 μ L of ES media. All cell types
849 were seeded at 5×10^4 cells per well, except for *Bmpr1a*^{-/-} cells, that were seeded at 6E04 per
850 well). For assays ran during differentiation, cells were seeded, the 3 days before the assay, onto
851 fibronectin-coated fibronectin-coated plates (1:100, Merck, UK), in 300 μ L of N2B27media. All
852 cell types were seeded at 2.4E04 cells per well, except for *Bmpr1a*^{-/-} cells, that were seeded at
853 3.2E04 cells per well.

854 On the day of the assay, cells were carefully washed twice with assay media and then left with a
855 final volume of the 600 μ L per well. The plate was then equilibrated on a non-CO₂ incubator at
856 37°C for 30 min. The assay media consisted in unbuffered DMEM (D5030 – Sigma, UK), that
857 was supplemented on the day of the assay according to the test performed. For the OCR
858 measurements the assay media was supplemented with 0.5 g.L⁻¹ of glucose (Sigma, UK) and 2
859 mM of L-glutamine (Life Technologies, UK), while for the ECAR measurements the media was
860 supplemented with 1 mM of Sodium Pyruvate and 2 mM of L-glutamine (both from Life
861 Technologies, UK), pH 7.4 at 37°C.

862 The protocol for the assay consisted of 4 baseline measurements and 3 measurements after
863 each compound addition. Compounds (all from Sigma, UK) used in OCR and ECAR assays
864 were prepared in the supplemented assay media. For the OCR assay, test the following
865 compounds were added: 1 mM Pyruvate (Pyr), 2.5 μ M oligomycin (OM), 300 nM Carbonyl
866 cyanide-4-(trifluoromethoxy) phenylhydrazone (FCCP) and a mixture of rotenone and antimycin
867 A at 6 μ M each (R&A). For the ECAR assay, the following compounds were added: 2.5 mM and
868 10 mM of glucose, 2.5 μ M of oligomycin (OM), and a 50 mM of 2-deoxyglucose (2-DG).
869 Each of the experiments was performed in 3 times, with 5 biological replicates of each cell type.
870 For background correction measurements, 4 wells were left without cells (A1, B4, C3 and D6).
871 Both ECAR and OCR measurements were performed on the same plate. The assay parameters
872 for both tests were calculated following the Seahorse assay report generator (Agilent
873 Technologies, UK).
874 At the end of the assay, cells were fixed and stained with Hoechst. Both OCR and ECAR were
875 normalised to cell number, determined by manual cell counts using Fiji software. The
876 normalisation of the data was processed on Wave Desktop software (Agilent Technologies, UK)
877 and data exported to Prism 8 (GraphPad) for statistical analysis.

878 **Analysis of mitochondrial membrane potential ($\Delta\psi$ m) and mitochondrial ROS**

879 Quantitative analysis of $\Delta\psi$ m and mitochondrial ROS was performed by flow cytometry. Cells
880 were grown in pluripotency or differentiating conditions, as described above. Cells were
881 dissociated and pelleted to obtain 2E05 cells per sample for the staining procedure.

882 For TMRM staining in single cells from early mouse epiblasts, embryos were dissected at E5.5
883 and cultured overnight in the presence or absence of caspase inhibitors. On the following
884 morning, to avoid misleading readings, epiblasts were isolated initially by an enzymatic
885 treatment with of 2.5% pancreatin, 0.5% trypsin and 0.5% polyvinylpyrrolidone (PVP40) - all from
886 Sigma-Aldrich- to remove the visceral endoderm (VE). Embryos were treated during 8 min at
887 4°C, followed by 2 min at RT. The VE was then peeled with the forceps and the extraembryonic
888 ectoderm removed to isolate the epiblasts. Up to 16 epiblasts were pooled per 600 μ L of

889 Accutase (Sigma-Aldrich) for dissociation into single cells prior to staining. Reaction was
890 stopped with equal volume of FCS and cells subjected to TMRM staining.

891 Cells were loaded with 10 nM of the Nernstian probe tetramethylrhodamin methyl ester
892 perchlorate (TMRM, Sigma), prepared in N2B27 media. After incubating for 15 min at 37°C, cells
893 were pelleted again and re-suspended in flow cytometry (FC) buffer (3% FCS in DPBS). Sytox
894 blue (1:1000, Invitrogen, UK) was used as viability staining. Stained cell suspensions were
895 analysed in BD LSRII flow cytometer operated through FACSDiva software (Becton Dickinson
896 Biosciences, UK). For TMRM fluorescence detection the yellow laser was adjusted for excitation
897 at $\lambda=562$ nm, capturing the emission light at $\lambda=585$ nm for TMRM. In the case of GFP-labelled
898 cell lines, for GFP fluorescence detection the blue laser was adjusted for excitation at $\lambda=488$ nm,
899 capturing the emission light at $\lambda=525$ nm. Results were analysed in FlowJo vX10.0.7r2.

900 Qualitative analysis of $\Delta\psi_m$ was performed by confocal microscopy. Wild-type and *Bmpr1a*^{-/-}
901 cells were grown in fibronectin-coated glass coverslips. On the third day of differentiation, cells
902 were loaded with 200 nM MitoTracker Red probe (Life Technologies), prepared in N2B27 media,
903 for 15 min at 37°C. Cells were then washed with DPBS and fixed with 3.7% formaldehyde for
904 subsequent immunocytochemical staining of total mitochondria mass, with TOMM20 antibody.
905 For the analysis of mitochondrial ROS, cells were grown in differentiating conditions and stained
906 on the third day of culture. Briefly, 2E05 cells of each cell line were resuspended in 200 μ L of 5
907 μ M solution of MitoSOX (Invitrogen, UK) prepared in N2B27 media. Cells were incubated at
908 37°C for 15 min, and then resuspended in FC buffer. MitoSOX fluorescence was analysed with
909 the violet laser adjusted for excitation at $\lambda=405$ nm, capturing the emission light at $\lambda=610$ nm.
910 Sytox blue was used as viability staining.

911 **Immunofluorescence**

912 Cells were washed with DPBS and fixed with 3.7% formaldehyde (Sigma, UK) in N2B27, for 15
913 min at 37°C. Permeabilization of the cell membranes was done with 0.4% Triton X-100 in DPBS
914 (DPBS-Tx), at RT with agitation. Blocking step with 5% BSA in DPBS-Tx 0.1% was performed
915 for 30 min, at RT with agitation. Mitochondria were labelled with TOMM20 antibody (1:100,

916 Santa Cruz Biotechnologies). Dead cells were labelled with cleaved caspase-3 antibody (1:400,
917 CST) and NANOG antibody was used to mark pluripotent cells (1:100, eBioscience). Secondary
918 antibodies were Alexa Fluor (1:600, Invitrogen). Primary antibody incubation was performed
919 overnight at 4°C and secondary antibody incubation during 45 min, together with Hoechst to
920 stain nuclei (1:1000, ThermoScientific), at RT and protected from light. In both cases antibodies
921 were diluted in blocking solution. Three 10 min washes with DPBS-Tx 0.1% were performed
922 between each critical step and before mounting with Vectashield medium (Vector Laboratories).

923 Samples were imaged with a Zeiss LSM780 confocal microscope (Zeiss, UK) and processed
924 with Fiji software⁶². Mitochondria stainings were imaged with a 63x/1.4 Oil objective. For
925 samples stained with TOMM20 antibody and MitoTracker Red, Z-stacks were acquired and
926 processed for deconvolution using Huygens software (Scientific Volume Imaging, <https://svi.nl/>).

927 Samples stained with cleaved caspase-3 were imaged with 20x/0.8 air objective. Imaging and
928 deconvolution analysis were performed with the support and advice from Mr. Stephen Rothery
929 from the Facility for Imaging by Light Microscopy (FILM) at Imperial College London.

930 Embryo immunofluorescent staining for p-rpS6, OPA1 and DDIT3 (CHOP) markers was
931 performed as follows. Cultured embryos were fixed in 4% PFA in DPBS containing 0.01% Triton
932 and 0.1% Tween 20 during 20 min at RT. Permeabilization of the membranes was done during
933 10 min in DPBS with 0.5% Triton. Embryos were blocked in 5% BSA in DPBS with 0.25% Triton
934 during 45 min. Incubation with primary antibodies - CHOP (1:500, CST- 2895S), OPA1 (1:100,
935 BD Biosciences - 612606) and p-rpS6 (CST - 5364) - was done overnight at 4°C in 2.5% BSA in
936 DPBS with 0.125% Triton. On the following morning, hybridisation with secondary antibodies
937 Alexa Fluor 568 and Alexa Fluor 488 (diluted 1:600 in DPBS with 2.5% BSA and 0.125% Triton)
938 was done next during 1h at RT. Hoechst was also added to this mixture to stain nuclei (1:1000,
939 Invitrogen). Three 10 min washes with filtered DPBS-Tx 0.1% were performed between each
940 critical step. All steps were done with gentle agitation.

941 Embryos were imaged in embryo dishes (Nunc) in a drop of Vectashield using Zeiss LSM780
942 confocal microscope at 40x/1.3 oil objective.

943 Further details about image acquisition and processing are specified in the Supplementary
944 Methods file “Imaging equipment and settings.docx”

945 **Western Blotting**

946 Cells were washed in DPBS and lysed with Laemmli lysis buffer (0.05 M Tris- HCl at pH 6.8, 1%
947 SDS, 10% glycerol, 0.1% β -mercaptoethanol in distilled water). Total protein quantification was
948 done using BCA assay (Thermo Scientific, UK) and samples (15 μ g of protein per lane) were
949 loaded into 12% Bis-Tris protein gels (BioRad). Resolved proteins were transferred into
950 nitrocellulose membranes (GE Healthcare). The following primary antibodies were incubated
951 overnight at 4°C: rabbit anti-TOMM20 (1:1000, CST - 42406), rabbit anti- α -Tubulin (1:1000,
952 CST- 2144), mouse anti-mt-CO1 (1:2000, Abcam - 14705), rabbit anti-DRP1 (1:1000, CST-
953 8570), mouse anti-MFN1 (1:1000, Abcam - 57602), mouse anti-MFN2 (1:500, Abcam - 56889),
954 mouse anti-Vinculin (1:1000, Sigma - V9131), mouse anti-OPA1 (1:1000, BD Biosciences -
955 612606), rabbit anti-ATF4 (1:1000, CST-11815), rabbit anti- α -PCNA (1:1000, Abcam - 2426)
956 and rabbit anti-p-eIF2 α (Ser51, 1:1000, CST-9721). On the following morning, HRP-conjugated
957 secondary antibodies (Santa Cruz) were incubated for 1h at RT. Membranes were developed
958 with ECL reagents (Promega) and mounted in cassette for time-time-controlled exposure to film
959 (GE Healthcare).

960 **Bulk RNA-Seq and Single cell RNA-Seq**

961 For bulk RNA Seq in the competitive scenario between cells with different mtDNA, HB(24%) and
962 BG(95%) mESCs were grown separately or in co-culture. On the third day of culture cells were
963 dissociated and subjected to fluorescence activated cell sorting (FACS) to separate the cell
964 populations in co-culture. To control for eventual transcriptional changes due to the FACS
965 process, a mixture of the two separate populations was subjected to the same procedure as the
966 co-cultured samples. Total RNA isolation was then carried out using RNA extraction Kit (RNeasy
967 Mini Kit, Qiagen). PolyA selection/enrichment was the method adopted for library preparation,
968 using the NEB Ultra II RNA Prep Kit. Single end 50bp libraries were sequenced on Illumina
969 Hiseq 2500. Raw basecall files were converted to fastq files using Illumina’s bcl2fastq (version

970 2.1.7). Reads were aligned to the mouse genome (mm9) using Tophat2 version 2.0.11⁶³ with
971 default parameters. Mapped reads that fell on genes were counted using featureCounts from
972 Rsubread package⁶⁴. Generated count data were then used to identify differentially expressed
973 genes using DESeq2⁶⁵. Genes with very low read counts were excluded. Finally, Gene Set
974 Enrichment Analysis was performed using GSEA software^{66, 67} on pre-ranked list generated by
975 DESeq2.

976 To investigate the nature of cells eliminated by cell competition during early mouse
977 embryogenesis by means of Single Cell RNA-Sequencing (scRNA-seq), early mouse embryos
978 were dissected at E5.5 and cultured overnight in the presence or absence of caspase inhibitors.
979 On the following morning, embryos were dissociated with Accutase and subjected to single-cell
980 sorting into 384-well plates. Total RNA isolation was then carried out using a RNA extraction Kit
981 (RNeasy Mini Kit, Qiagen). scRNA-seq was performed using the Smart-seq2 protocol⁶⁸. PolyA
982 selection/enrichment with Ultra II Kit (NEB) was the method adopted for library preparation.

983 **Data processing, quality control and normalization**

984 We performed transcript quantification in our scRNA-seq data by running Salmon v0.8.2⁶⁹ in the
985 quasi-mapping-based mode. First, a transcriptome index was created from the mouse reference
986 (version GRCm38.p4) and ERCC spike-in sequences. Then, the quantification step was carried
987 out with the “quant” function, correcting for the sequence-specific biases (“--seqBias” flag) and
988 the fragment-level GC biases (“--gcBias” flag). Finally, the transcript level abundances were
989 aggregated to gene level counts. On the resulting raw count matrix including 1,495 cells, we
990 apply a quality control to exclude poor quality cells from downstream analyses.

991 For the quality control we used the following criteria: we identified the cells that have a \log_{10} total
992 number of reads equal to or greater than 4, a fraction of mapped reads equal to or greater than
993 0.8, a number of genes with expression level above 10 reads per million equal to or greater than
994 3000 and a fraction of reads mapped to endogenous genes equal to or greater than 0.5. This
995 resulted in the selection of 723 cells, which were kept for downstream analyses. Transcripts per
996 million (TPM) normalization (as estimated by Salmon) was used.

997 **Identification of highly variable genes and dimensionality reduction**

998 To identify highly variable genes (HVG), first we fitted a mean-total variance trend using the R
999 function “trendVar” and then the variance was decomposed into biological and technical
1000 components with the R function “decomposeVar”; both functions are included in the package
1001 “scran” (version 1.6.9 ⁷⁰).

1002 We considered HVGs those that have a biological component that is significantly greater than
1003 zero at a false discovery rate (Benjamini-Hochberg method) of 0.05. Then, we applied further
1004 filtering steps by keeping only genes that have an average expression greater to or equal than
1005 10 TPM and are significantly correlated with one another (function “correlatePairs” in “scran”
1006 package, FDR<0.05). This yielded 1921 genes, which were used to calculate a distance matrix
1007 between cells defined as $\sqrt{(1 - \rho)/2}$, where ρ is the Spearman’s correlation coefficient
1008 between cells. A 2D representation of the data was obtained with the UMAP package (version
1009 0.2.0.0 <https://cran.r-project.org/web/packages/umap/index.html>) using the distance matrix as
1010 input.

1011 **Cell clustering and connectivity analysis**

1012 To classify cells into different clusters, we ran hierarchical clustering on the distance matrix (see
1013 above; “hclust” function in R with ward.D2 aggregation method) followed by the dynamic hybrid
1014 cut algorithm (“cutreeDynamic” function in R package “dynamicTreeCut” ([https://CRAN.R-](https://CRAN.R-project.org/package=dynamicTreeCut)
1015 [project.org/package=dynamicTreeCut](https://CRAN.R-project.org/package=dynamicTreeCut)) version 1.63.1, with the hybrid method, a minimum
1016 cluster size of 35 cells and a “deepSplit” parameter equal to 0), which identified five clusters.
1017 Cells from different batches were well mixed across these five clusters (see Extended Data Fig.
1018 1), suggesting that the batch effect was negligible. The identity of the five clusters was
1019 established based on the expression of known marker genes of Epiblast, Visceral Endoderm
1020 and Extra-Embryonic Ectoderm, which were identified in a previous study⁵⁶. The expression
1021 levels of some of the top markers is plotted in Figure 1b.

1022 We performed a robustness analysis on the clustering by exploring in detail how the choices of
1023 genes, clustering parameters and algorithms affect the identity and the number of clusters. First,

1024 we quantified the cluster robustness by calculating Pearson's gamma and the Average
1025 silhouette width obtained with 100 random subsets of 60% of the highly variable genes and
1026 different values of the deepSplit parameter. While the robustness at deepSplit=0 and 1 is similar,
1027 for greater values of deepSplit (corresponding to less conservative clustering) the robustness
1028 rapidly declines (Extended Data Figure 2a). The clustering with deepSplit = 0 and 1 (the more
1029 robust choices) yield very similar results, the only difference being the splitting of the
1030 intermediate cluster in two subclusters (Extended Data Figure 2b).

1031 In addition to this, we also used Louvain clustering on the highly variable genes (resolution=0.3,
1032 k=20 with 20 principal components), which again produced very similar clusters.

1033 We quantified the connectivity between the clusters (using only CI-treated cells) with PAGA²²
1034 implemented in the python library scanpy (version 1.4.7)⁷¹. The analysis revealed that the three
1035 epiblast clusters are connected with each other while the two extra embryonic tissues (Visceral
1036 Endoderm and Extra Embryonic Ectoderm) are isolated (Extended Data Figure 2c).

1037 **Identification of a single-cell trajectory in the epiblast**

1038 We calculated a diffusion map ("DiffusionMap" function in the R package "destiny" version 2.6.2
1039 ²³ on the distance defined above on the epiblast cells from CI-treated embryos. The pseudotime
1040 coordinate was computed with the "DPT" function with the root cell in the winner epiblast cluster
1041 (identified by the function "tips" in the "destiny" package). Such pseudotime coordinate can be
1042 interpreted as a "losing score" for all the epiblast cells from the CI-treated embryos.

1043 We estimated the losing scores of the epiblast cells from DMSO-treated embryos by projecting
1044 such data onto the diffusion map previously calculated (function "dm_predict" in the destiny
1045 package). Finally, for each of the projected cells, we assigned the losing score as the average of
1046 the losing scores of the 10 closest neighbours in the original diffusion map (detected with the
1047 function "projection-dist" in the destiny package).

1048 While for the clustering and the trajectory analysis we used the highly variable genes computed
1049 from the whole dataset, we verified that all results concerning the separation between winner

1050 and loser epiblast cells (eg, clusters and losing score) remain unaffected if the highly variable
1051 genes are calculated using only the epiblast cells.

1052 **Mapping of data from epiblast cells onto published single-cell RNA seq datasets of** 1053 **epiblast from freshly isolated embryos**

1054 We compared the transcriptional profile of epiblast from embryos cultured in DMSO and CI with
1055 that of epiblast collected from freshly isolated embryos at different stages.

1056 To do this, we considered the dataset published in²⁶, which includes epiblast cells from embryos
1057 at the stages E5.5 (102 cells), E6.25 (130 cells) and E6.5 (288 cells). A diffusion map and a
1058 diffusion pseudotime coordinate were computed with these cells following the same procedure
1059 described in the section above (Extended Data Figure 2d-e). Then, we projected epiblast cells
1060 from CI and DMSO-treated embryos and we assigned to them a diffusion pseudotime coordinate
1061 as described above (Extended Data Figure 2f).

1062 **Differential gene expression analysis along the trajectory**

1063 To identify the genes that are differentially expressed along the trajectory, first we kept only
1064 genes that have more than 15 TPM in more than 10 cells (this list of genes is provided in
1065 Supplementary Table 4); then, we obtained the log-transformed expression levels of these
1066 genes (adding 1 as a pseudo-count to avoid infinities) as a function of the losing score and we
1067 fitted a generalized additive model to them (R function “gam” from “GAM” package version
1068 1.16.). We used the ANOVA test for parametric effect provided by the gam function to estimate a
1069 p-value for each tested gene. This yielded a list of 5,311 differentially expressed genes (FDR <
1070 0.01).

1071 Next, we looked for groups of differentially expressed genes that share similar expression
1072 patterns along the trajectory. To this aim, similarly to what we did when clustering cells, we
1073 calculated a correlation-based distance matrix between genes, defined as $\sqrt{(1 - \rho)/2}$, where ρ
1074 is the Spearman’s correlation coefficient between genes. Hierarchical clustering was then
1075 applied to this matrix (hclust function in R, with ward.D2 method) followed by the dynamic hybrid

1076 cut algorithm (dynamicTreeCut package) to define clusters (“cutreeDynamic” function in R with
1077 the hybrid method and a minimum cluster size of 100 genes and a deepSplit parameter equal to
1078 0). This resulted in the definition of four clusters, three of genes that decrease along the
1079 trajectory (merged together for the GO enrichment and the IPA analysis) and one of increasing
1080 genes (Extended Data Fig. 2d). IPA (QIAGEN Inc., [https://www.qiagenbio-](https://www.qiagenbioinformatics.com/products/ingenuity-pathway-analysis)
1081 [informatics.com/products/ingenuity-pathway-analysis](https://www.qiagenbioinformatics.com/products/ingenuity-pathway-analysis)), was run on all genes differentially
1082 expressed (FDR < 0.01) along the trajectory from winner to loser cells (see Fig. 2a-d and Fig.
1083 3a-c), using all the tested genes as a background (see Supplementary Table 4). This software
1084 generated networks, canonical pathways and functional analysis. The list of
1085 decreasing/increasing genes is provided in Supplementary Tables 1 and 2.

1086 **Analysis of Mitochondrial DNA heteroplasmy in single-cell RNA seq dataset**

1087 We used STAR (version 2.7⁷²) to align the transcriptome of the epiblast cells from CI-treated
1088 embryos (274) to the mouse reference genome (mm10). Only reads that uniquely mapped to the
1089 mitochondrial DNA (mtDNA) were considered. From these, we obtained allele counts at each
1090 mtDNA position with a Phred Quality Score greater than 33 using the samtools mpileup function.
1091 Next, we applied filters to remove cells and mtDNA positions with a low coverage. First, we
1092 removed cells with fewer than 2,000 mtDNA positions covered by more than 50 reads. Second,
1093 we removed positions having less than 50 reads in more than 50% of cells in each of the three
1094 epiblast clusters (winner, intermediate and loser). These two filters resulted in 259 cells and
1095 5,192 mtDNA positions (covered by ~700 reads per cell on average) being considered for further
1096 analyses.

1097 Starting from these cells and positions, we applied an additional filter to keep only positions with
1098 a sufficiently high level of heteroplasmy. To this aim, for each position with more than 50 reads
1099 in a cell, we estimated the heteroplasmy as:

$$H = 1 - f_{max}$$

1100 where f_{max} is the frequency of the most common allele. We kept only positions with $H > 0.01$ in at
1101 least 10 cells.

1102 Finally, using generalized additive models (see above), we identified the positions whose
1103 heteroplasmy H changes as a function of the cells' losing score in a statistically significant way.
1104 We found a total of eleven significant positions (FDR < 0.001), six of them in the *mt-Rnr1* gene
1105 and five in the *mt-Rnr2* gene. All of these positions have a higher level of heteroplasmy in loser
1106 cells (see Fig. 6b-g and Extended Data Fig. 6f-k). The results remain substantially unaltered if
1107 the Spearman's rank correlation test (in alternative to the generalized additive models) is used.
1108 For the barplot shown in Fig. 6h and the correlation heatmaps in Fig. 6i and Extended Data Fig.
1109 6l, we took into account only cells that covered with more than 50 reads all the significant
1110 positions in the *mt-Rnr1* gene (215 cells, Fig. 6h-6i) or in both the *mt-Rnr1* and *mt-Rnr2* genes
1111 (214 cells, Extended Data Fig. 6l).

1112 As a negative control, we repeated the analysis described above using the ERCC spike-ins
1113 added to each cell. As expected, none of the positions was statistically significant, which
1114 suggested that our procedure is robust against sequence errors introduced during PCR
1115 amplification.

1116 We also performed the mtDNA heteroplasmy analysis in cells from the Visceral Endoderm and
1117 the Extra-Embryonic Ectoderm in both DMSO and CI conditions: none of these cells have a
1118 mtDNA heteroplasmy higher than 0.01 in the 11 significant positions identified within *mt-Rnr1*
1119 and *mt-Rnr2* in loser epiblast cells, and the reference allele is always the most common. This
1120 reinforces the hypothesis that such variants are specific to loser epiblast cells and are not
1121 resulting from contamination.

1122 To test the reliability of our heteroplasmy estimations, we used the RNA-seq data from two of the
1123 mtDNA cell lines (BG and HB, see Figure 7), for which the heteroplasmy was measured also by
1124 ARMS-qPCR. To do so, first we downloaded the fasta files of the two mtDNA cell lines from
1125 <https://www.ncbi.nlm.nih.gov/nucleotide/KC663619.1> and
1126 <https://www.ncbi.nlm.nih.gov/nucleotide/KC663620.1>, then we identified the mtDNA positions that
1127 differ from the BL6 reference genome. Finally, on these different positions, the heteroplasmy H

1128 was computed as explained above. The values of heteroplasmy we found with our
1129 computational analysis were very close to those estimated by ARMS-qPCR (~17% from RNA-
1130 seq data vs ~21% measured by ARMS-qPCR; and ~93% from RNA-seq data vs ~97% by
1131 measured by ARMS-qPCR).

1132 **Common features of scRNA-seq and bulk RNA-seq datasets**

1133 Differential expression analysis between the co-cultured winner HB(24%) and loser cell line
1134 BG(95%) was performed using the package EdgeR version 3.20.9⁷³.
1135 Batches were specified in the argument of the function model.matrix. We fitted a quasi-likelihood
1136 negative binomial generalized log-linear model (with the function glmQLFit) to the genes that
1137 were filtered by the function filterByExpr (with default parameter). These genes were used as
1138 background for the gene enrichment analysis.
1139 We set a FDR of 0.001 as a threshold for significance. The enrichment analysis for both the
1140 scRNA-seq and bulk RNA-seq datasets were performed using the tool g:Profiler⁷⁴. The list of
1141 up-regulated, down-regulated and background genes related to the DE analysis for the bulk
1142 RNA-seq dataset are provided in the Supplementary Tables 5, 6 and 7.

1143 **Quantification and Statistical Analysis**

1144 Box plots show lower quartile (Q1, 25th percentile), median (Q2, 50th percentile) and upper
1145 quartile (Q3, 75th percentile). Box length refers to interquartile range (IQR, Q3-Q1). The upper
1146 whisker marks the minimum between the maximum value in the dataset and the IQR times 1.5
1147 from Q3 (Q3+1.5 x IQR), while the lower whisker marks the maximum between the minimum
1148 value in the dataset and IQR times 1.5 from Q1 (Q1-1.5 x IQR). Outliers are shown outside the
1149 interval defined by box and whiskers as individual points.
1150 Flow cytometry data was analysed with FlowJo Software.
1151 Western blot quantification was performed using Image Studio Lite (LI-COR). Protein expression
1152 levels were normalised to loading controls vinculin or α -tubulin.
1153 The quantification of the DDIT3 and OPA1 expression in embryos was done by two distinct
1154 methods. DDIT3 expression was quantified by counting the number of epiblast cells with positive

1155 staining in the embryos of each group. The expression of OPA1 was quantified on Fiji software
1156 as the mean fluorescence across a 10 pixel width line drawn on the basal cytoplasm of each cell
1157 with high or low p-rpS6 fluorescence intensity, as specified in⁷. min of 8 cells were quantified per
1158 condition (high vs low mTOR activity) in each embryo. Six embryos treated with CI were
1159 analysed. Mean grey values of OPA1 fluorescence for each epiblast cell are pooled on the same
1160 graph.

1161 Normalisation of data from metabolic flux analysis with Seahorse was performed using Wave
1162 Desktop software (Agilent Technologies, UK) and data exported to Prism 8 (GraphPad) for
1163 statistical analysis.

1164 The statistical analysis of the results was performed using GraphPad Prism version 8.0.0 for
1165 Mac (GraphPad Software, San Diego, California USA). Data was tested for normality using
1166 Shapiro-Wilk normality test. Parametric or non-parametric statistical tests were applied
1167 accordingly. Details about the test used in each of the experiments are specified in figure
1168 legends. Statistical significance was considered with a confidence interval of 0.05%. n.s., non-
1169 significant; * $p < 0.05$; ** $p < 0.01$; *** $p < 0.001$.

1170 **Data Availability**

1171 Data were analysed with standard programs and packages, as detailed above. Authors can
1172 confirm that all relevant data are included in the paper and/ or its supplementary information
1173 files. Source data for Figures 2-5,7 and for Extended Data Figures 4-5, 7-8 are provided with
1174 the paper. RNA-seq raw as well as processed data are available through ArrayExpress,
1175 accession numbers E-MTAB-8640, for scRNA-seq data, and E-MTAB-8692, for bulk RNA-seq
1176 data.

1177

1178 **Code Availability**

1179 All code that was used in this study is available upon request.

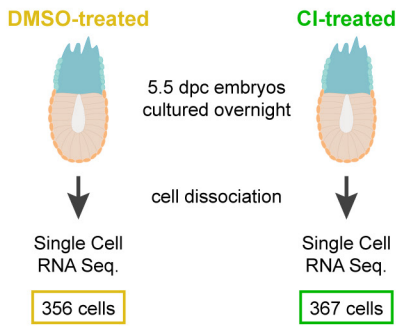
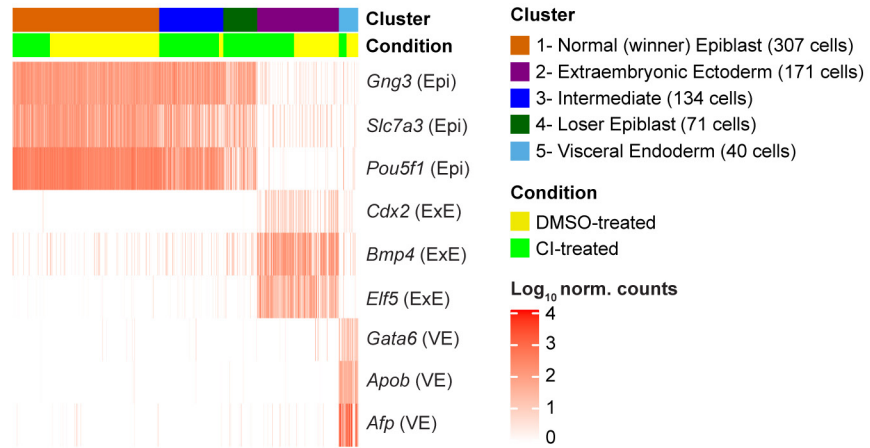
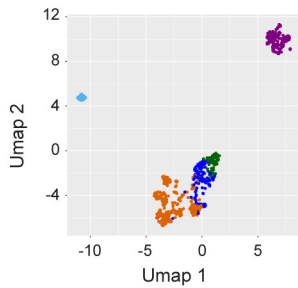
1180 References

- 1181 1. Bowling, S., Lawlor, K. & Rodriguez, T.A. Cell competition: the winners and losers of
1182 fitness selection. *Development* **146** (2019).
- 1183 2. Diaz-Diaz, C. & Torres, M. Insights into the quantitative and dynamic aspects of Cell
1184 Competition. *Curr Opin Cell Biol* **60**, 68-74 (2019).
- 1185 3. Madan, E., Gogna, R. & Moreno, E. Cell competition in development: information from
1186 flies and vertebrates. *Curr Opin Cell Biol* **55**, 150-157 (2018).
- 1187 4. Morata, G. & Ripoll, P. Minutes: mutants of drosophila autonomously affecting cell
1188 division rate. *Dev Biol* **42**, 211-221 (1975).
- 1189 5. Claveria, C., Giovinazzo, G., Sierra, R. & Torres, M. Myc-driven endogenous cell
1190 competition in the early mammalian embryo. *Nature* **500**, 39-44 (2013).
- 1191 6. Sancho, M. *et al.* Competitive interactions eliminate unfit embryonic stem cells at the
1192 onset of differentiation. *Dev Cell* **26**, 19-30 (2013).
- 1193 7. Bowling, S. *et al.* P53 and mTOR signalling determine fitness selection through cell
1194 competition during early mouse embryonic development. *Nat Commun* **9**, 1763 (2018).
- 1195 8. Diaz-Diaz, C. *et al.* Pluripotency Surveillance by Myc-Driven Competitive Elimination of
1196 Differentiating Cells. *Dev Cell* **42**, 585-599 e584 (2017).
- 1197 9. Hashimoto, M. & Sasaki, H. Epiblast Formation by TEAD-YAP-Dependent Expression
1198 of Pluripotency Factors and Competitive Elimination of Unspecified Cells. *Dev Cell* **50**,
1199 139-154 e135 (2019).
- 1200 10. Lima, A., Burgstaller, J., Sanchez-Nieto, J.M. & Rodriguez, T.A. The Mitochondria and
1201 the Regulation of Cell Fitness During Early Mammalian Development. *Curr Top Dev Biol*
1202 **128**, 339-363 (2018).
- 1203 11. Zhou, W. *et al.* HIF1alpha induced switch from bivalent to exclusively glycolytic
1204 metabolism during ESC-to-EpiSC/hESC transition. *EMBO J* **31**, 2103-2116 (2012).
- 1205 12. Khrapko, K. *et al.* Mitochondrial mutational spectra in human cells and tissues. *Proc Natl*
1206 *Acad Sci U S A* **94**, 13798-13803 (1997).
- 1207 13. Allio, R., Donega, S., Galtier, N. & Nabholz, B. Large Variation in the Ratio of
1208 Mitochondrial to Nuclear Mutation Rate across Animals: Implications for Genetic
1209 Diversity and the Use of Mitochondrial DNA as a Molecular Marker. *Mol Biol Evol* **34**,
1210 2762-2772 (2017).
- 1211 14. Burgstaller, J.P., Johnston, I.G. & Poulton, J. Mitochondrial DNA disease and
1212 developmental implications for reproductive strategies. *Mol Hum Reprod* **21**, 11-22
1213 (2015).
- 1214 15. Gorman, G.S. *et al.* Mitochondrial diseases. *Nat Rev Dis Primers* **2**, 16080 (2016).
- 1215 16. Burgstaller, J.P. *et al.* MtDNA segregation in heteroplasmic tissues is common in vivo
1216 and modulated by haplotype differences and developmental stage. *Cell Rep* **7**, 2031-2041
1217 (2014).
- 1218 17. Johnston, I.G. *et al.* Stochastic modelling, Bayesian inference, and new in vivo
1219 measurements elucidate the debated mtDNA bottleneck mechanism. *Elife* **4**, e07464
1220 (2015).
- 1221 18. Latorre-Pellicer, A. *et al.* Regulation of Mother-to-Offspring Transmission of mtDNA
1222 Heteroplasmy. *Cell Metab* (2019).
- 1223 19. Lee, H.S. *et al.* Rapid mitochondrial DNA segregation in primate preimplantation
1224 embryos precedes somatic and germline bottleneck. *Cell Rep* **1**, 506-515 (2012).
- 1225 20. Zhang, H., Burr, S.P. & Chinnery, P.F. The mitochondrial DNA genetic bottleneck:
1226 inheritance and beyond. *Essays Biochem* **62**, 225-234 (2018).

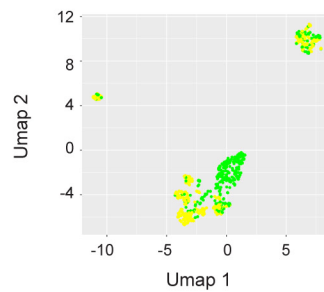
- 1227 21. Sharpley, M.S. *et al.* Heteroplasmy of mouse mtDNA is genetically unstable and results
1228 in altered behavior and cognition. *Cell* **151**, 333-343 (2012).
- 1229 22. Wolf, F.A. *et al.* PAGA: graph abstraction reconciles clustering with trajectory inference
1230 through a topology preserving map of single cells. *Genome Biol* **20**, 59 (2019).
- 1231 23. Angerer, P. *et al.* destiny: diffusion maps for large-scale single-cell data in R.
1232 *Bioinformatics* **32**, 1241-1243 (2016).
- 1233 24. Kramer, A., Green, J., Pollard, J., Jr. & Tugendreich, S. Causal analysis approaches in
1234 Ingenuity Pathway Analysis. *Bioinformatics* **30**, 523-530 (2014).
- 1235 25. Haghverdi, L., Buttner, M., Wolf, F.A., Buettner, F. & Theis, F.J. Diffusion pseudotime
1236 robustly reconstructs lineage branching. *Nature methods* **13**, 845-848 (2016).
- 1237 26. Cheng, S. *et al.* Single-Cell RNA-Seq Reveals Cellular Heterogeneity of Pluripotency
1238 Transition and X Chromosome Dynamics during Early Mouse Development. *Cell Rep* **26**,
1239 2593-2607 e2593 (2019).
- 1240 27. Topf, U., Wrobel, L. & Chacinska, A. Chatty Mitochondria: Keeping Balance in Cellular
1241 Protein Homeostasis. *Trends Cell Biol* **26**, 577-586 (2016).
- 1242 28. Melber, A. & Haynes, C.M. UPR(mt) regulation and output: a stress response mediated
1243 by mitochondrial-nuclear communication. *Cell Res* **28**, 281-295 (2018).
- 1244 29. Munch, C. The different axes of the mammalian mitochondrial unfolded protein response.
1245 *BMC Biol* **16**, 81 (2018).
- 1246 30. Zhao, Q. *et al.* A mitochondrial specific stress response in mammalian cells. *EMBO J* **21**,
1247 4411-4419 (2002).
- 1248 31. Nargund, A.M., Pellegrino, M.W., Fiorese, C.J., Baker, B.M. & Haynes, C.M.
1249 Mitochondrial import efficiency of ATFS-1 regulates mitochondrial UPR activation.
1250 *Science* **337**, 587-590 (2012).
- 1251 32. Quiros, P.M., Mottis, A. & Auwerx, J. Mitonuclear communication in homeostasis and
1252 stress. *Nat Rev Mol Cell Biol* **17**, 213-226 (2016).
- 1253 33. Mouchiroud, L. *et al.* The NAD(+)/Sirtuin Pathway Modulates Longevity through
1254 Activation of Mitochondrial UPR and FOXO Signaling. *Cell* **154**, 430-441 (2013).
- 1255 34. Saveljeva, S. *et al.* Endoplasmic reticulum stress-mediated induction of SESTRIN 2
1256 potentiates cell survival. *Oncotarget* **7**, 12254-12266 (2016).
- 1257 35. Yun, J. & Finkel, T. Mitohormesis. *Cell Metab* **19**, 757-766 (2014).
- 1258 36. Chen, H. *et al.* Mitofusins Mfn1 and Mfn2 coordinately regulate mitochondrial fusion and
1259 are essential for embryonic development. *J Cell Biol* **160**, 189-200 (2003).
- 1260 37. Prudent, J. & McBride, H.M. The mitochondria-endoplasmic reticulum contact sites: a
1261 signalling platform for cell death. *Curr Opin Cell Biol* **47**, 52-63 (2017).
- 1262 38. Smirnova, E., Griparic, L., Shurland, D.L. & van der Bliek, A.M. Dynamin-related
1263 protein Drp1 is required for mitochondrial division in mammalian cells. *Mol Biol Cell* **12**,
1264 2245-2256 (2001).
- 1265 39. Favaro, G. *et al.* DRP1-mediated mitochondrial shape controls calcium homeostasis and
1266 muscle mass. *Nat Commun* **10**, 2576 (2019).
- 1267 40. Quiros, P.M. *et al.* Multi-omics analysis identifies ATF4 as a key regulator of the
1268 mitochondrial stress response in mammals. *J Cell Biol* **216**, 2027-2045 (2017).
- 1269 41. Restelli, L.M. *et al.* Neuronal Mitochondrial Dysfunction Activates the Integrated Stress
1270 Response to Induce Fibroblast Growth Factor 21. *Cell Rep* **24**, 1407-1414 (2018).
- 1271 42. Richter, U. *et al.* A mitochondrial ribosomal and RNA decay pathway blocks cell
1272 proliferation. *Curr Biol* **23**, 535-541 (2013).
- 1273 43. Moullan, N. *et al.* Tetracyclines Disturb Mitochondrial Function across Eukaryotic
1274 Models: A Call for Caution in Biomedical Research. *Cell Rep* **10**, 1681-1691 (2015).

- 1275 44. Kauppila, J.H.K. *et al.* A Phenotype-Driven Approach to Generate Mouse Models with
1276 Pathogenic mtDNA Mutations Causing Mitochondrial Disease. *Cell Rep* **16**, 2980-2990
1277 (2016).
- 1278 45. Fan, W. *et al.* A mouse model of mitochondrial disease reveals germline selection against
1279 severe mtDNA mutations. *Science* **319**, 958-962 (2008).
- 1280 46. Stewart, J.B. *et al.* Strong purifying selection in transmission of mammalian
1281 mitochondrial DNA. *PLoS Biol* **6**, e10 (2008).
- 1282 47. Freyer, C. *et al.* Variation in germline mtDNA heteroplasmy is determined prenatally but
1283 modified during subsequent transmission. *Nat Genet* **44**, 1282-1285 (2012).
- 1284 48. Ludwig, L.S. *et al.* Lineage Tracing in Humans Enabled by Mitochondrial Mutations and
1285 Single-Cell Genomics. *Cell* **176**, 1325-1339 e1322 (2019).
- 1286 49. Chinnery, P.F. & Hudson, G. Mitochondrial genetics. *Br Med Bull* **106**, 135-159 (2013).
- 1287 50. Floros, V.I. *et al.* Segregation of mitochondrial DNA heteroplasmy through a
1288 developmental genetic bottleneck in human embryos. *Nat Cell Biol* **20**, 144-151 (2018).
- 1289 51. Burr, S.P., Pezet, M. & Chinnery, P.F. Mitochondrial DNA Heteroplasmy and Purifying
1290 Selection in the Mammalian Female Germ Line. *Dev Growth Differ* **60**, 21-32 (2018).
- 1291 52. Rajasimha, H.K., Chinnery, P.F. & Samuels, D.C. Selection against pathogenic mtDNA
1292 mutations in a stem cell population leads to the loss of the 3243A-->G mutation in blood.
1293 *Am J Hum Genet* **82**, 333-343 (2008).
- 1294 53. Ellis, S.J. *et al.* Distinct modes of cell competition shape mammalian tissue
1295 morphogenesis. *Nature* **569**, 497-502 (2019).
- 1296 54. Kucinski, I., Dinan, M., Kolahgar, G. & Piddini, E. Chronic activation of JNK JAK/STAT
1297 and oxidative stress signalling causes the loser cell status. *Nat Commun* **8**, 136 (2017).
- 1298 55. Kon, S. *et al.* Cell competition with normal epithelial cells promotes apical extrusion of
1299 transformed cells through metabolic changes. *Nat Cell Biol* **19**, 530-541 (2017).
- 1300 56. Scialdone, A. *et al.* Resolving early mesoderm diversification through single-cell
1301 expression profiling. *Nature* **535**, 289-293 (2016).
- 1302 57. Zappia, L. & Oshlack, A. Clustering trees: a visualization for evaluating clusterings at
1303 multiple resolutions. *GigaScience* **7**, giy083 (2018).
- 1304 58. Scialdone, A. *et al.* Computational assignment of cell-cycle stage from single-cell
1305 transcriptome data. *Methods* **85**, 54-61 (2015).
- 1306 59. Fischer, M. Census and evaluation of p53 target genes. *Oncogene* **36**, 3943-3956 (2017).
- 1307 60. Ran, F.A. *et al.* Genome engineering using the CRISPR-Cas9 system. *Nat Protoc* **8**,
1308 2281-2308 (2013).
- 1309 61. Czechanski, A. *et al.* Derivation and characterization of mouse embryonic stem cells from
1310 permissive and nonpermissive strains. *Nat Protoc* **9**, 559-574 (2014).
- 1311 62. Schindelin, J. *et al.* Fiji: an open-source platform for biological-image analysis. *Nat*
1312 *Methods* **9**, 676-682 (2012).
- 1313 63. Kim, D. *et al.* TopHat2: accurate alignment of transcriptomes in the presence of
1314 insertions, deletions and gene fusions. *Genome Biol* **14**, R36 (2013).
- 1315 64. Liao, Y., Smyth, G.K. & Shi, W. The R package Rsubread is easier, faster, cheaper and
1316 better for alignment and quantification of RNA sequencing reads. *Nucleic Acids Res* **47**,
1317 e47 (2019).
- 1318 65. Love, M.I., Huber, W. & Anders, S. Moderated estimation of fold change and dispersion
1319 for RNA-seq data with DESeq2. *Genome Biol* **15**, 550 (2014).
- 1320 66. Mootha, V.K. *et al.* PGC-1alpha-responsive genes involved in oxidative phosphorylation
1321 are coordinately downregulated in human diabetes. *Nat Genet* **34**, 267-273 (2003).
- 1322 67. Subramanian, A. *et al.* Gene set enrichment analysis: a knowledge-based approach for
1323 interpreting genome-wide expression profiles. *Proc Natl Acad Sci U S A* **102**, 15545-
1324 15550 (2005).

- 1325 68. Picelli, S. *et al.* Smart-seq2 for sensitive full-length transcriptome profiling in single cells.
1326 *Nat Methods* **10**, 1096-1098 (2013).
- 1327 69. Patro, R., Duggal, G., Love, M.I., Irizarry, R.A. & Kingsford, C. Salmon provides fast
1328 and bias-aware quantification of transcript expression. *Nat Methods* **14**, 417-419 (2017).
- 1329 70. Lun, A.T., McCarthy, D.J. & Marioni, J.C. A step-by-step workflow for low-level
1330 analysis of single-cell RNA-seq data with Bioconductor. *F1000Res* **5**, 2122 (2016).
- 1331 71. Wolf, F.A., Angerer, P. & Theis, F.J. SCANPY: large-scale single-cell gene expression
1332 data analysis. *Genome Biol* **19**, 15 (2018).
- 1333 72. Dobin, A. *et al.* STAR: ultrafast universal RNA-seq aligner. *Bioinformatics* **29**, 15-21
1334 (2013).
- 1335 73. Robinson, M.D., McCarthy, D.J. & Smyth, G.K. edgeR: a Bioconductor package for
1336 differential expression analysis of digital gene expression data. *Bioinformatics* **26**, 139-
1337 140 (2010).
- 1338 74. Reimand, J., Arak, T. & Vilo, J. g:Profiler--a web server for functional interpretation of
1339 gene lists (2011 update). *Nucleic Acids Res* **39**, W307-315 (2011).
- 1340

Fig. 1**a****b****c****Clusters:**

- 1- Normal (winner) Epiblast (78 CI, 229 DMSO)
- 2- Extraembryonic Ectoderm (77 CI, 94 DMSO)
- 3- Intermediate (125 CI, 9 DMSO)
- 4- Loser Epiblast (71 CI, 0 DMSO)
- 5- Visceral Endoderm (16 CI, 24 DMSO)

d**Conditions**

- DMSO-treated (356 cells)
- CI-treated (367 cells)

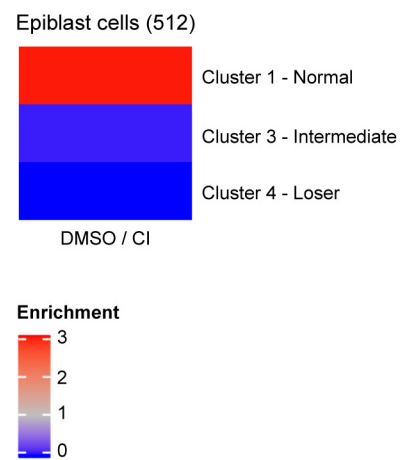
e

Fig. 2

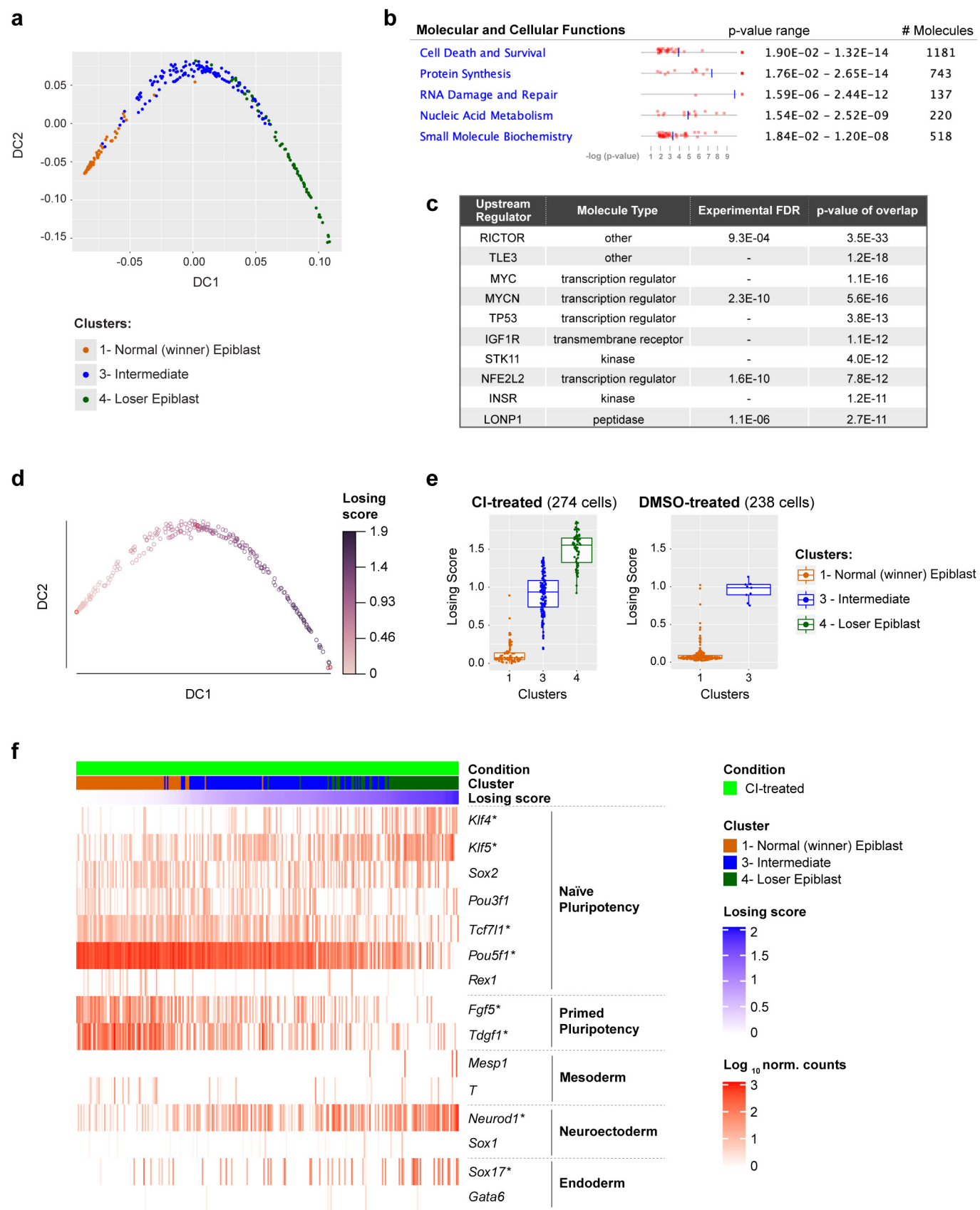


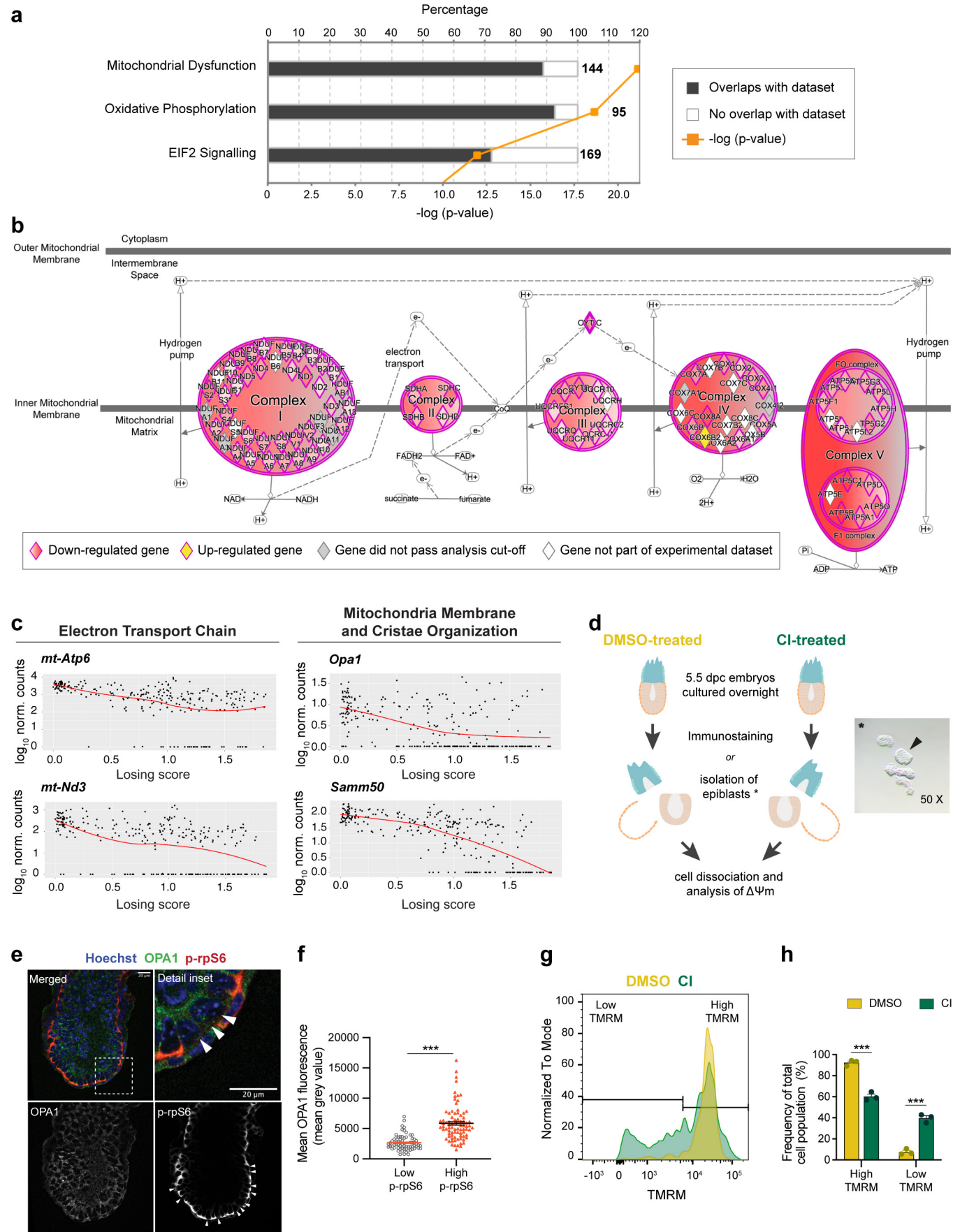
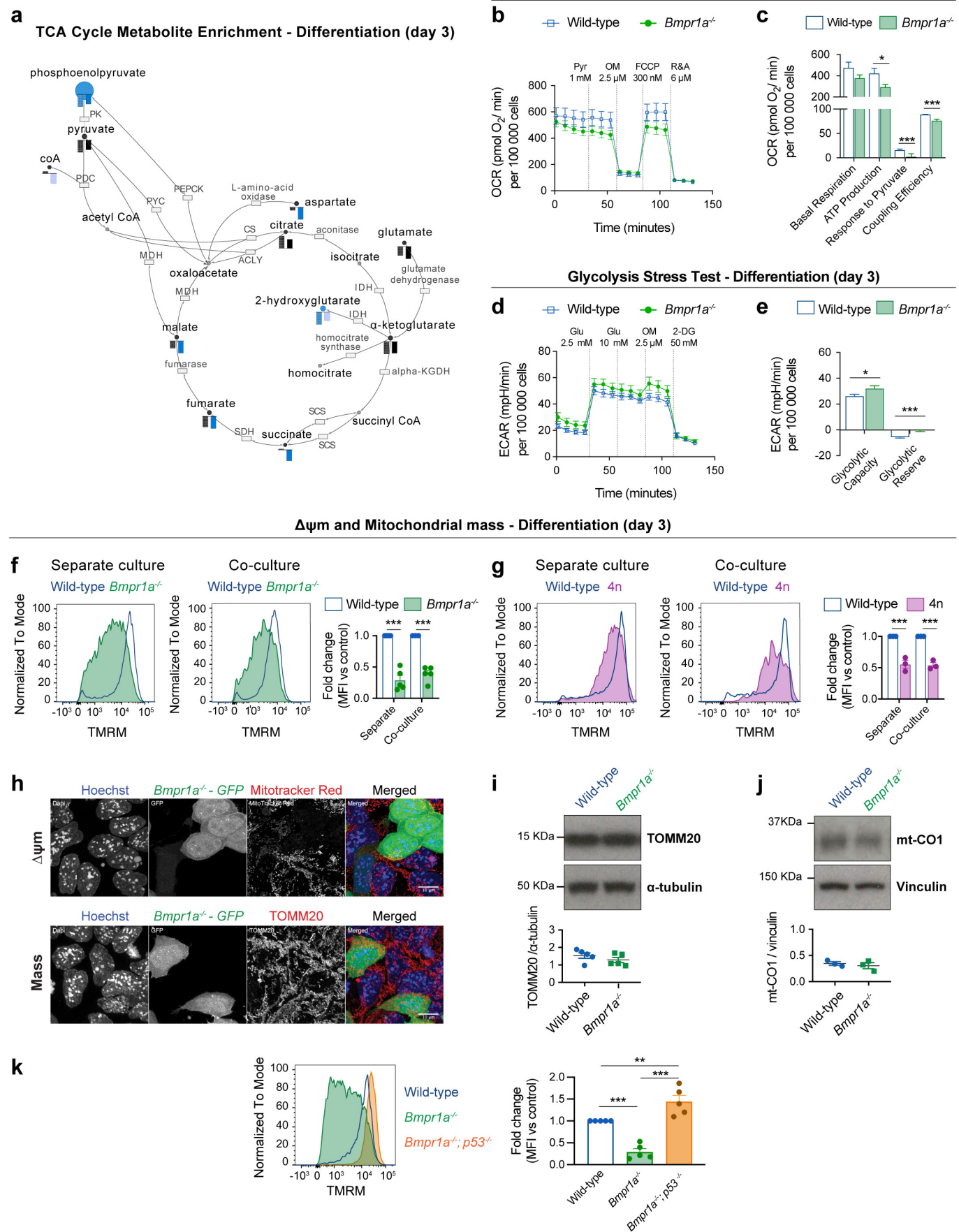
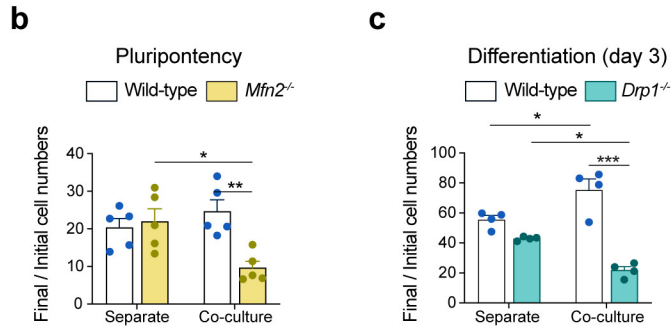
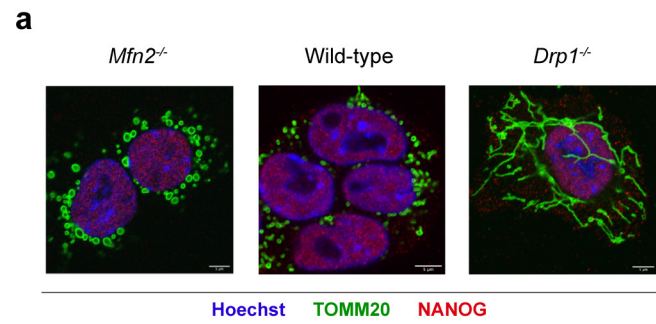
Fig. 3

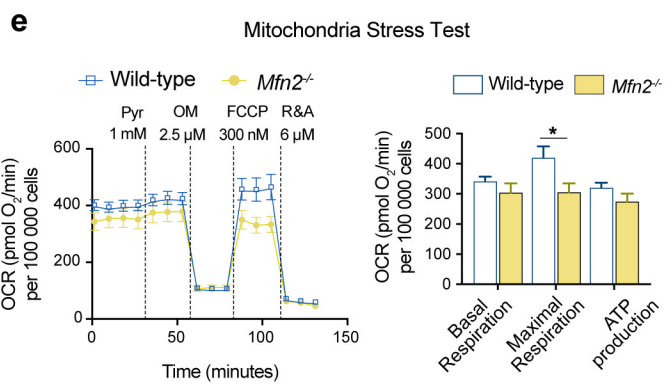
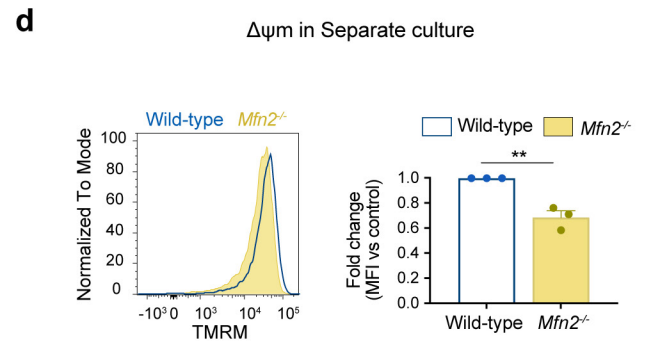
Fig. 4

Mitochondrial shape - Pluripotency

Cell competition assays



Metabolic profile of *Mfn2^{-/-}* cells - Pluripotency



Metabolic profile of *Drp1^{-/-}* cells - Differentiation (day 3)

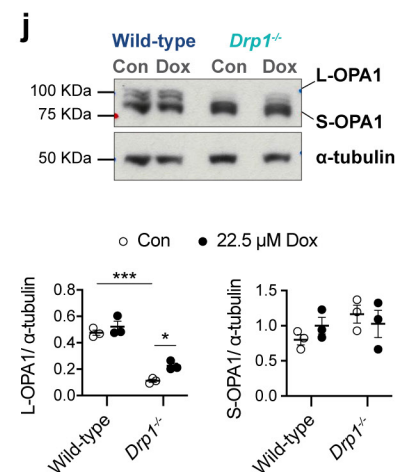
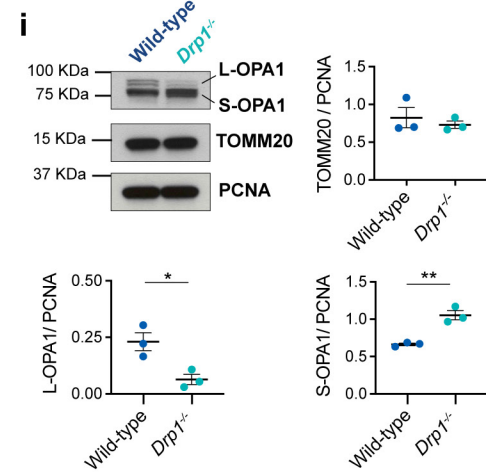
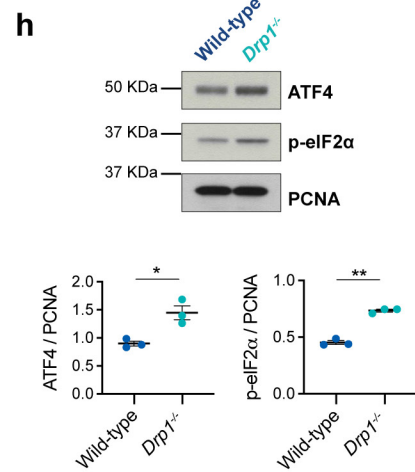
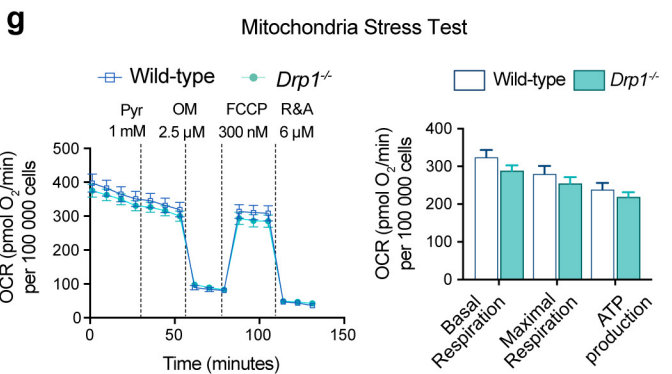
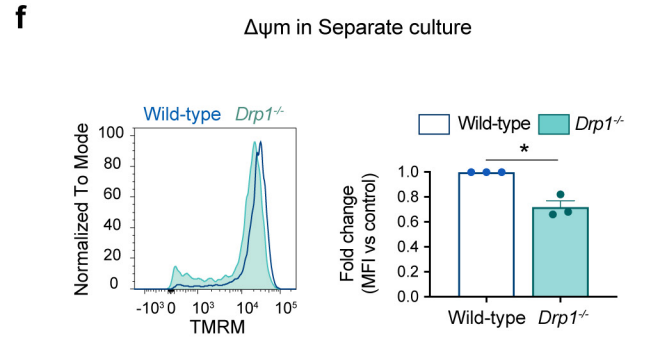


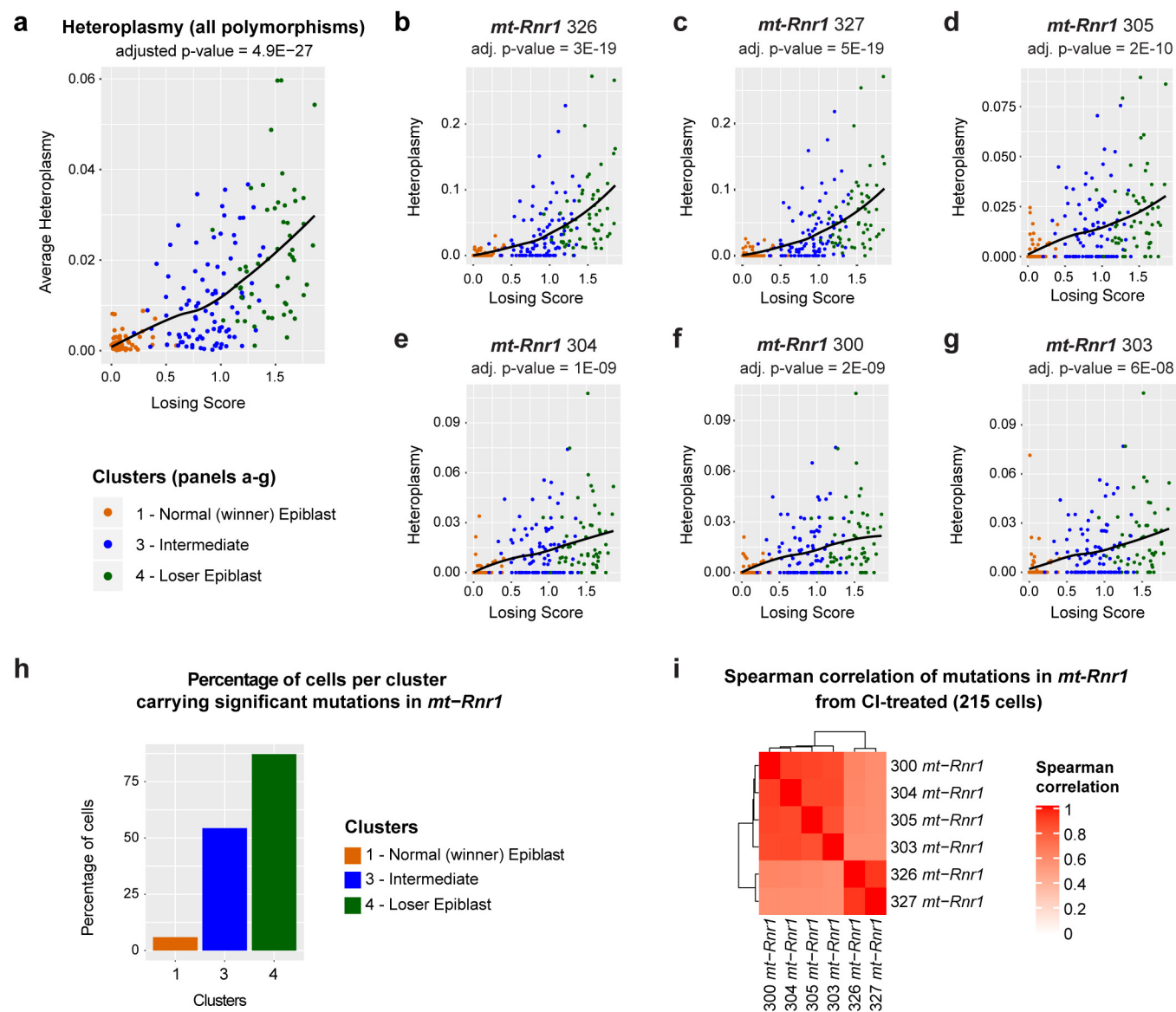
Fig. 6

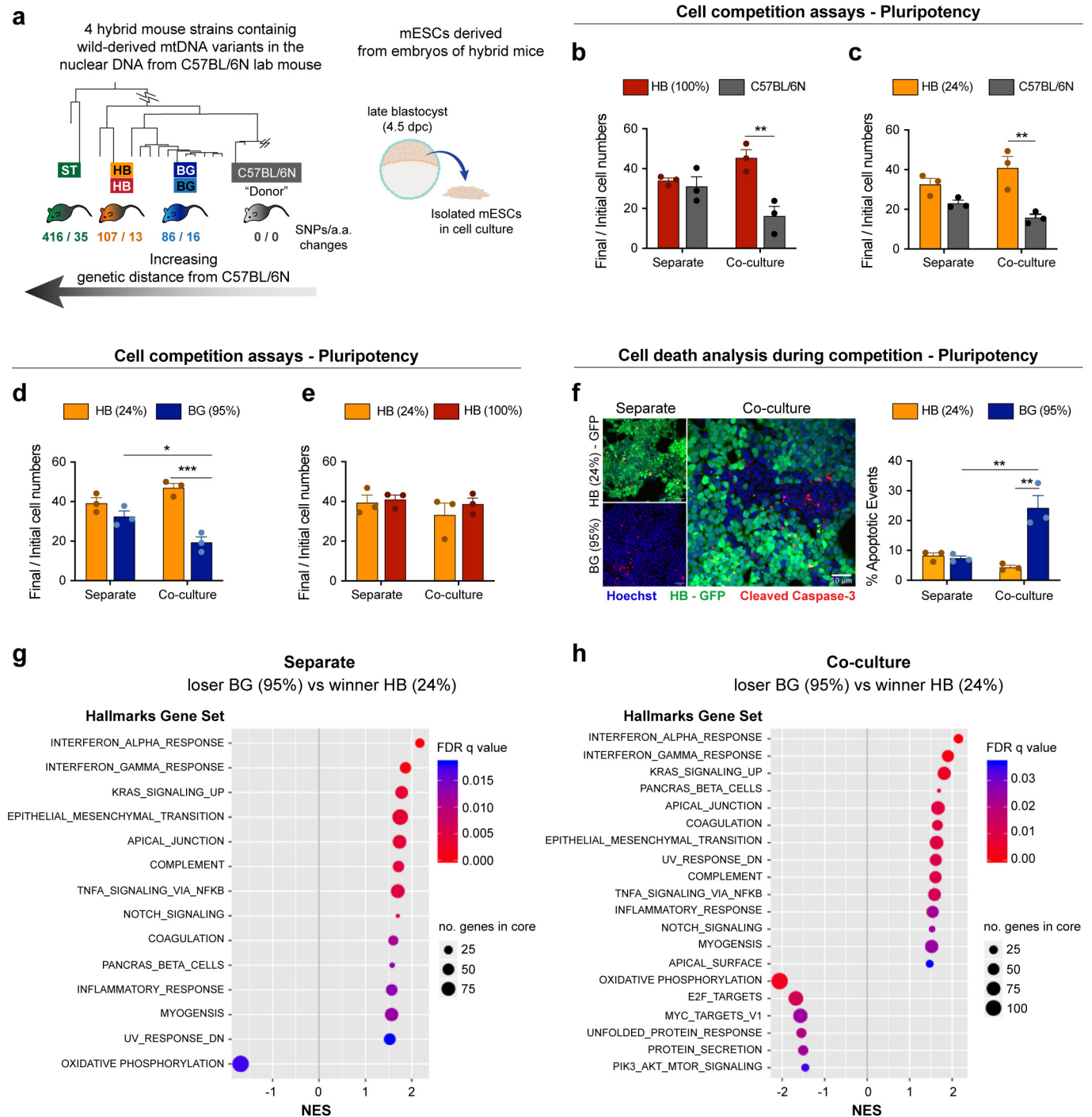
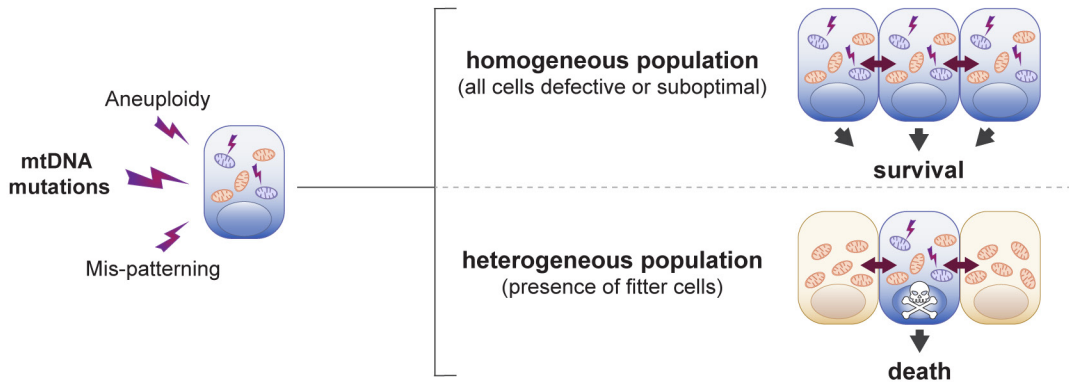
Fig. 7

Fig. 8

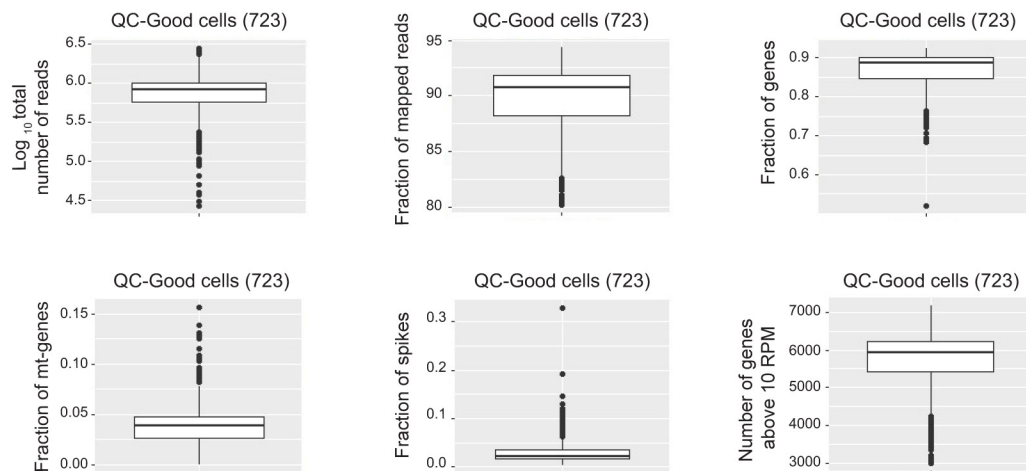
Mitochondria-centered Cell Fitness



Extended Data Fig. 1

a

Selection criteria for quality control (QC) of cells



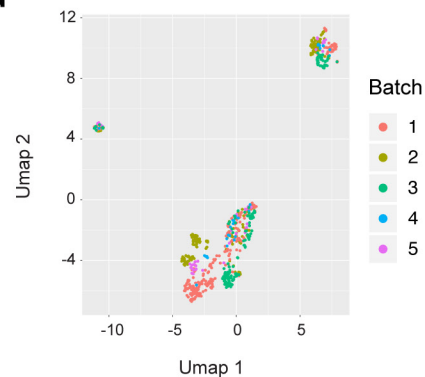
b

Condition\Batch	1	2	3	4	5
CI-treated	136	105	86	16	24
DMSO	132	110	78	15	21

c

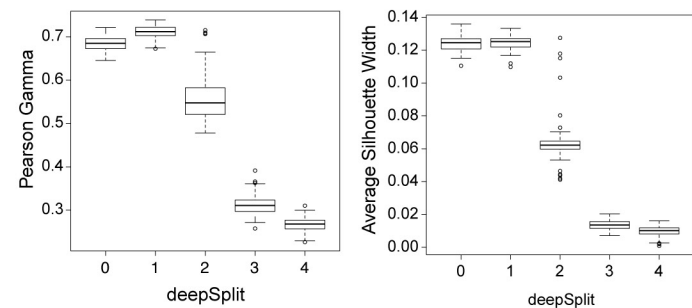
Cluster/Batch	1	2	3	4	5
1	147	81	57	7	15
2	45	65	44	7	10
3	46	34	35	13	6
4	23	18	21	2	7
5	7	17	7	2	7

d



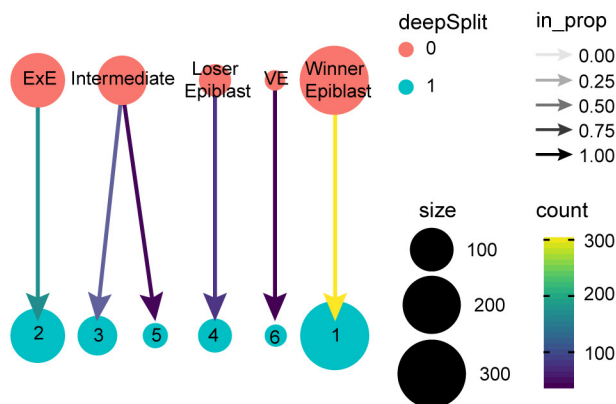
e

Cluster robustness



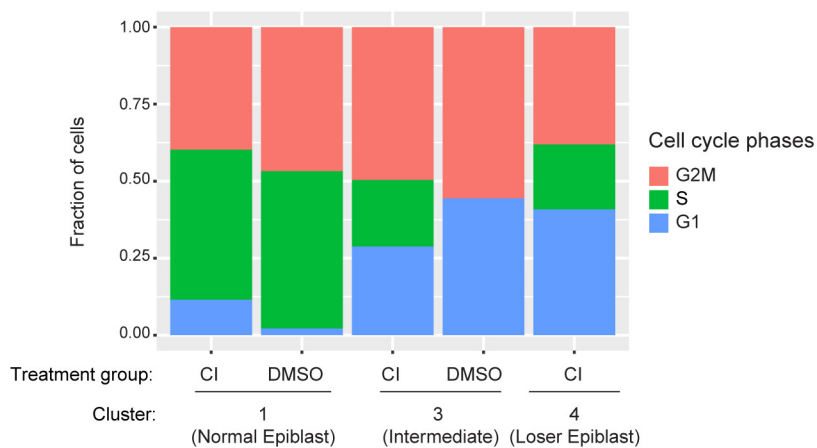
f

deepSplit clustering

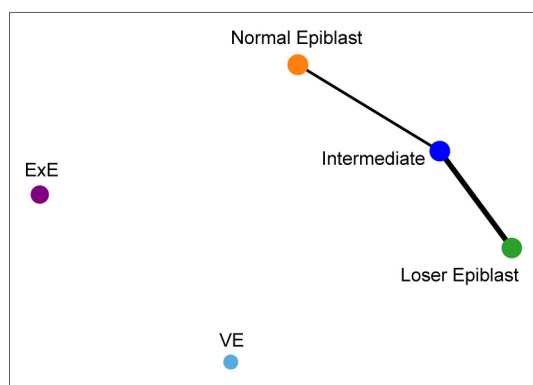


Extended Data Fig. 2

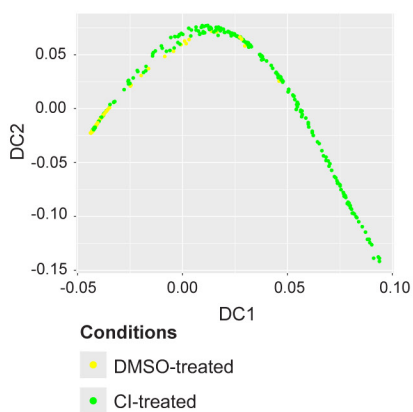
a



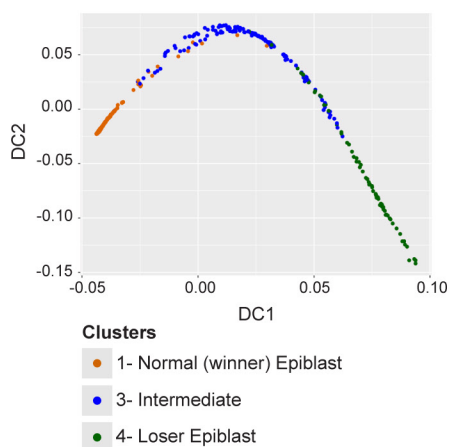
b



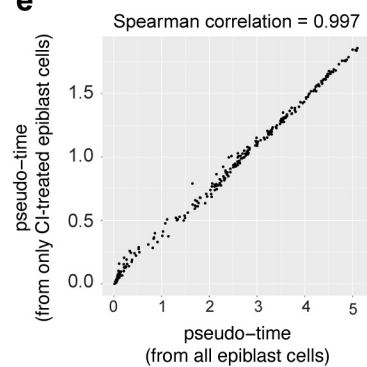
c



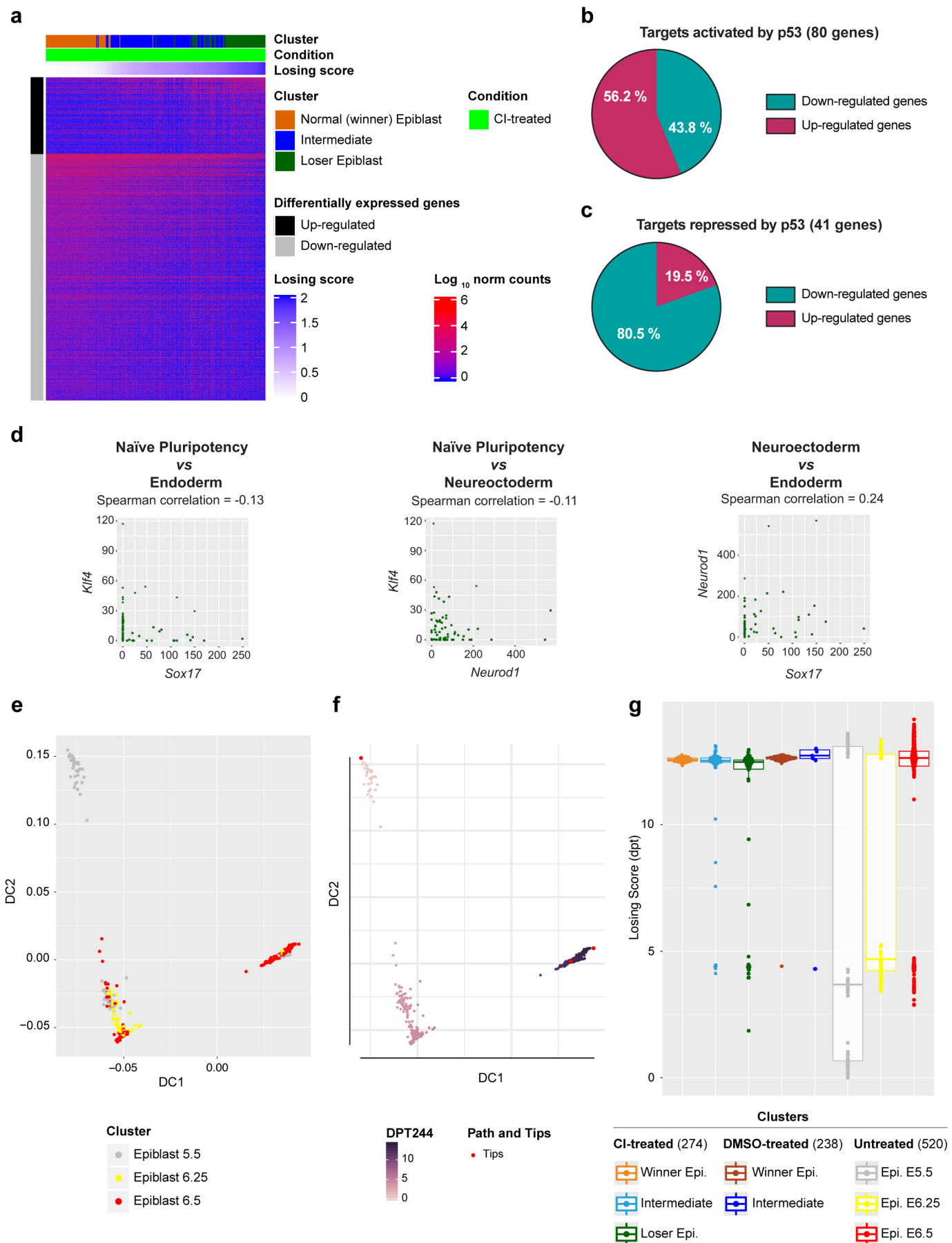
d



e

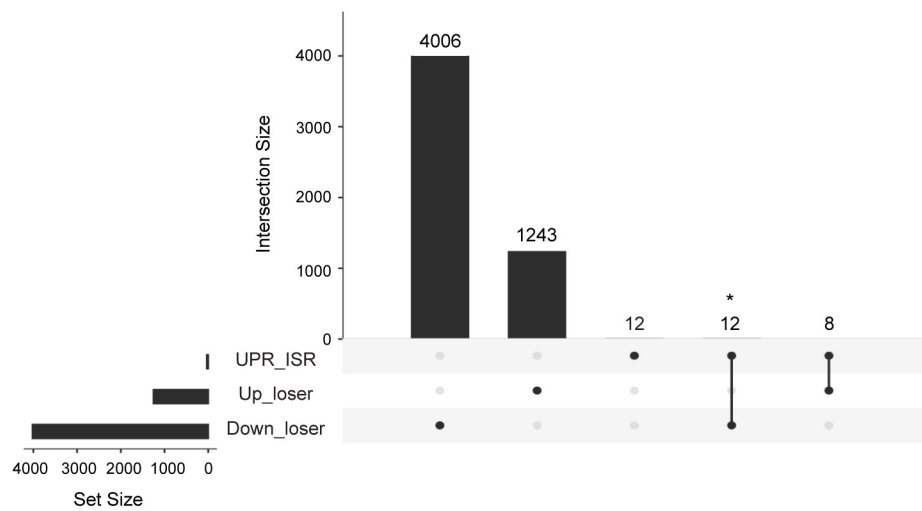


Extended Data Fig. 3



Extended Data Fig. 4

a



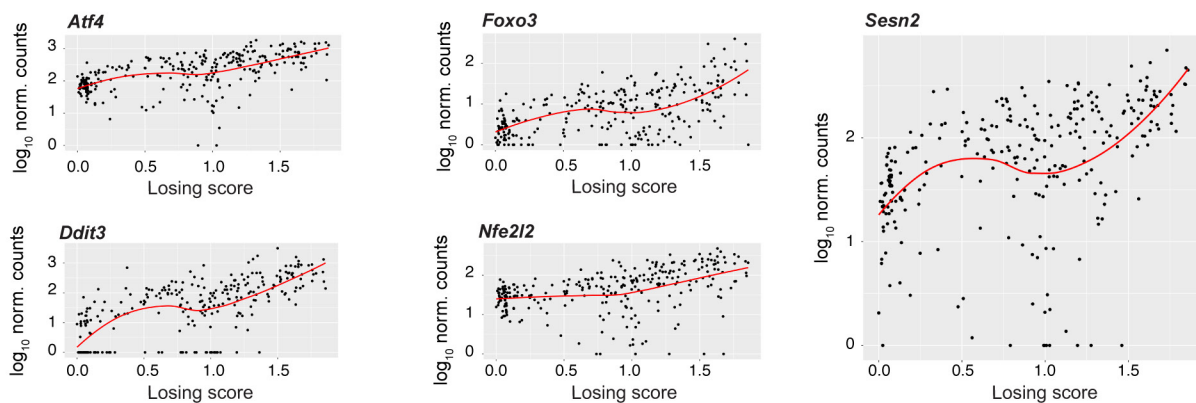
b

Gene	FDR	Rank
<i>Ddit3</i>	4.63E-39	2
<i>Atf3</i>	6.08E-27	22
<i>Atf4</i>	2.14E-23	31
<i>Foxo3</i>	2.69E-22	37
<i>Ppp1r15a</i>	8.33E-18	68
<i>Eif2ak3</i>	7.17E-13	150
<i>Nfe2l2</i>	1.55E-10	207
<i>Gdf15</i>	5.53E-08	333

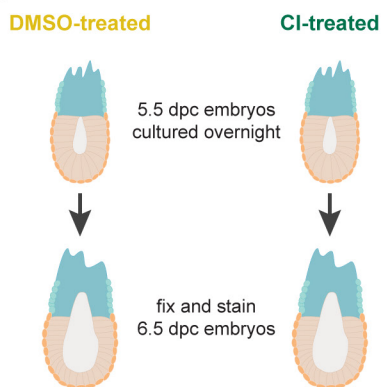
c

Gene	FDR	Rank
<i>Mthfd1l</i>	2.54E-35	147
<i>Hspe1</i>	8.71E-34	164
<i>Cat</i>	2.44E-30	219
<i>Hspd1</i>	6.93E-13	1262
<i>Sod2</i>	1.25E-10	1551
<i>Hsph1</i>	4.48E-10	1655
<i>Lonp1</i>	1.08E-06	2348
<i>Eif2a</i>	1.49E-06	2382
<i>Mthfd2</i>	1.31E-05	2693
<i>Hspa4</i>	2.84E-05	2790
<i>Cth</i>	2.53E-03	3677
<i>Nrf1</i>	2.86E-03	3698

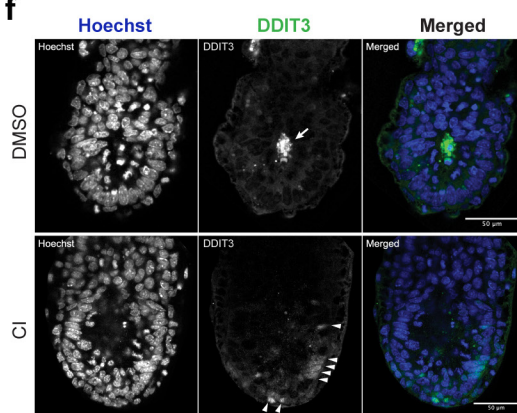
d



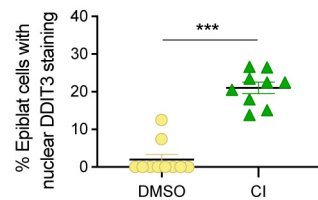
e



f

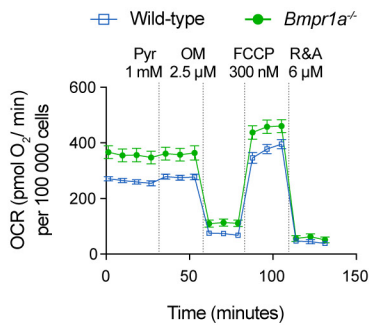


g

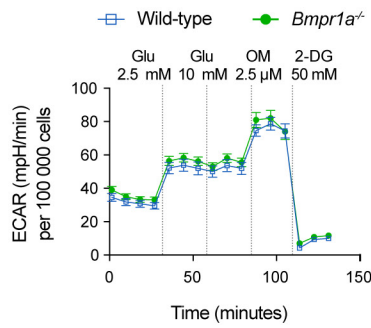


Extended Data Fig. 5

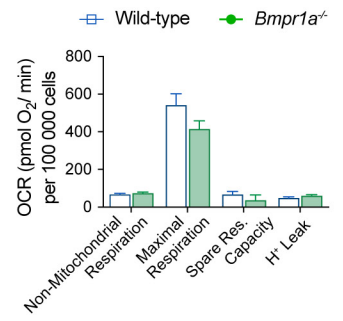
a Mitochondria Stress Test - Pluripotency



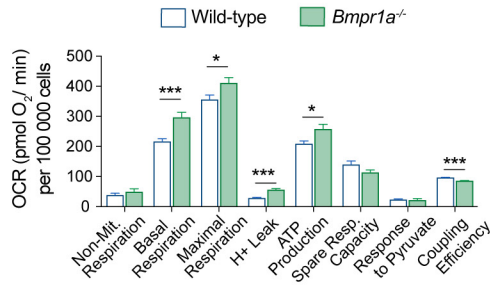
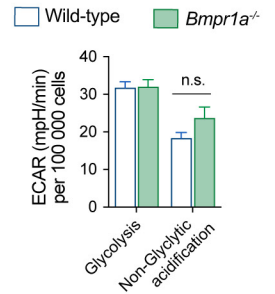
b Glycolysis Stress Test - Pluripotency



c Mitochondria Stress Test - Differentiation (day 3)

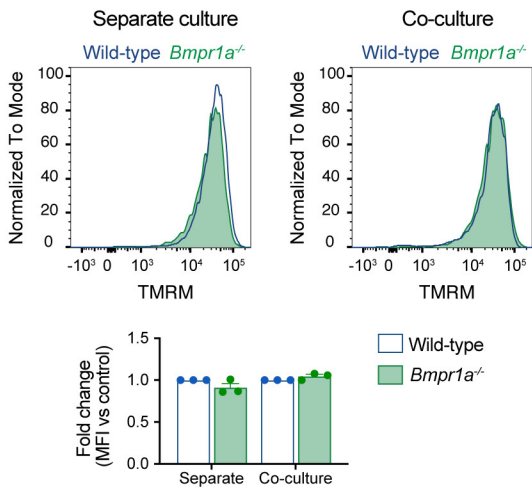


d Glycolysis Stress Test - Differentiation (day 3)

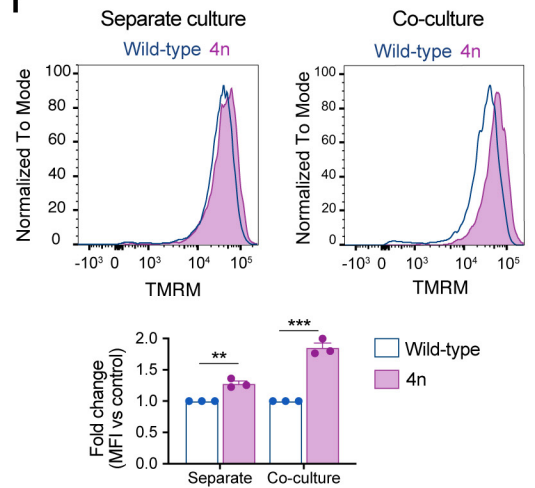


Δψm - Pluripotency

e

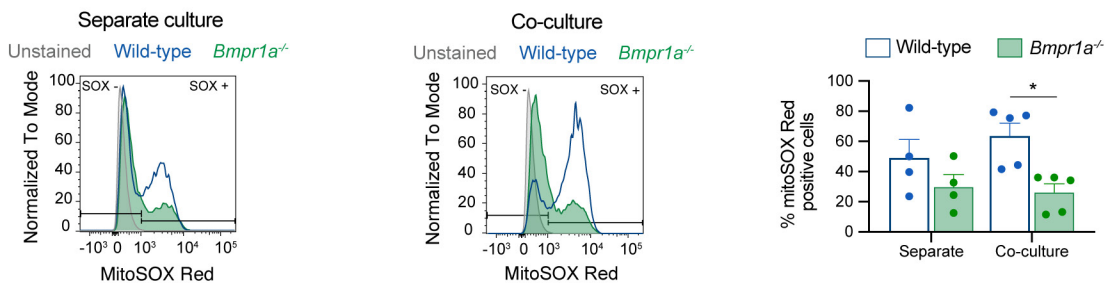


f



Mitochondrial ROS - Differentiation (day 3)

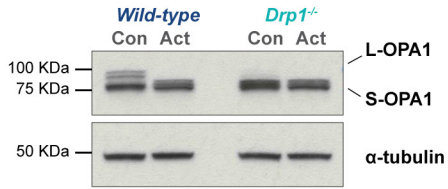
g



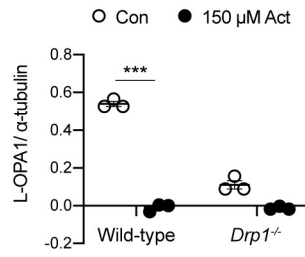
Extended Data Fig. 6

Act treatment at Differentiation day 3 (6h)

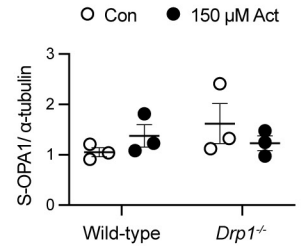
a



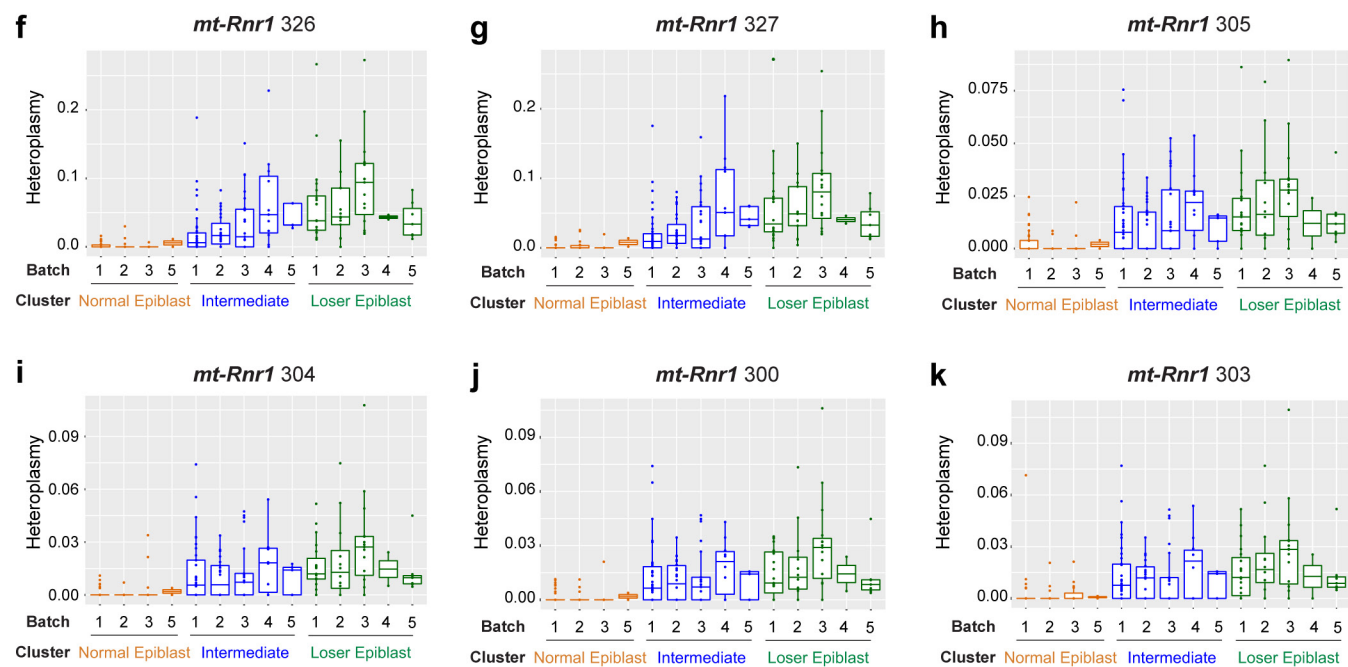
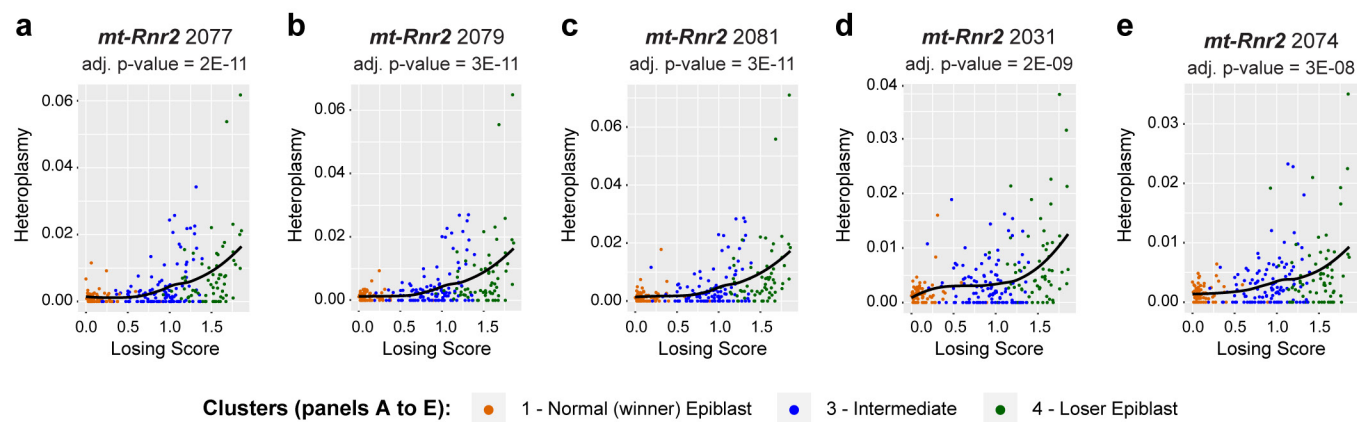
b



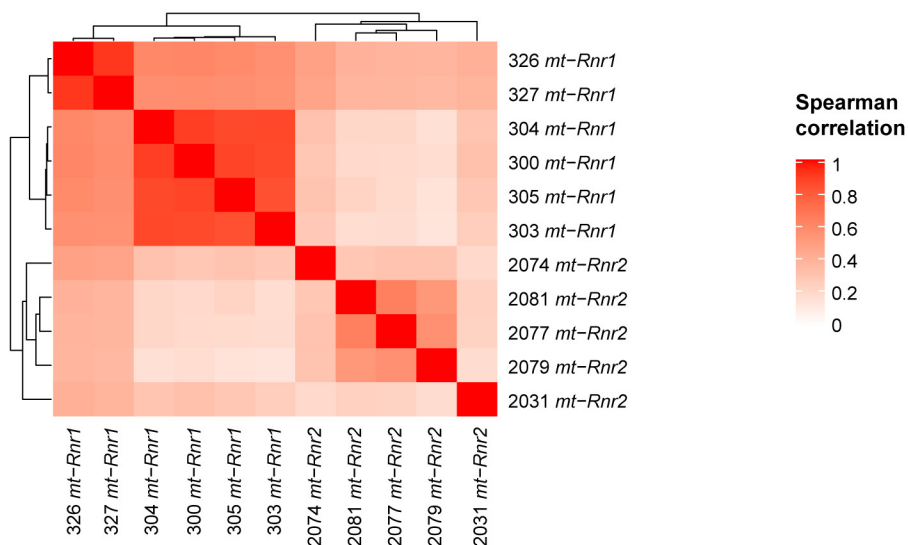
c



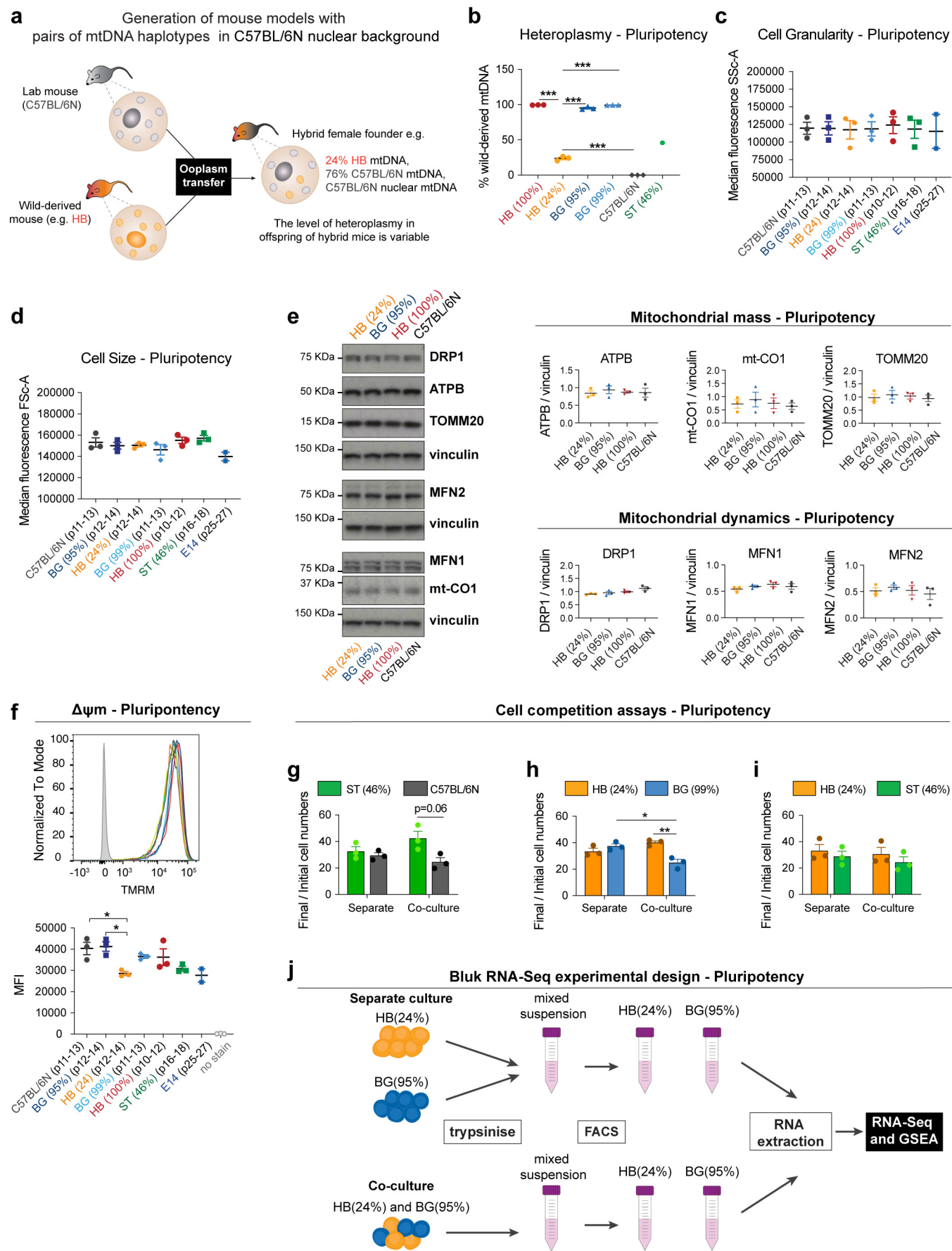
Extended Data Fig. 7



l Spearman correlation of mutations within *mt-Rnr1* and *mt-Rnr2* from CI-treated (214 cells)



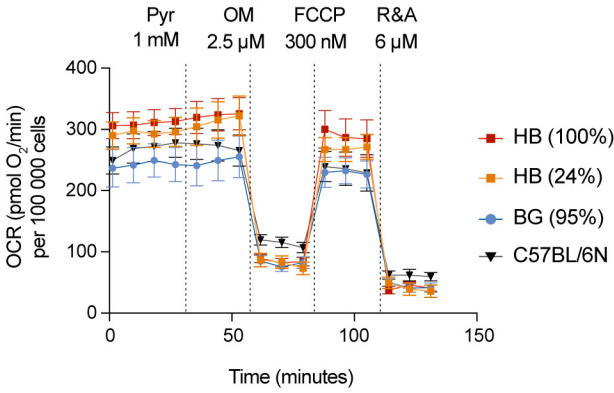
Extended Data Fig. 8



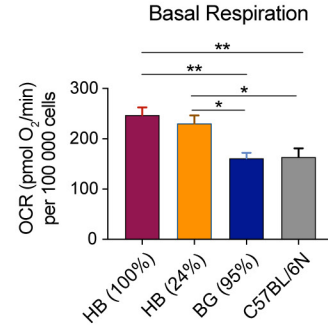
Extended Data Fig. 9

Mitochondria Stress Test - Pluripotency

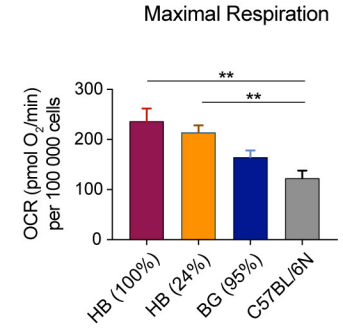
a



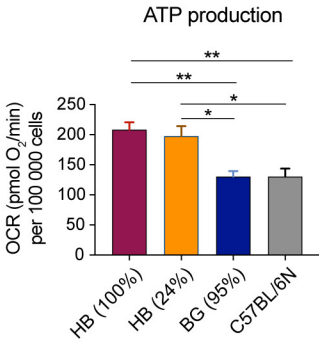
b



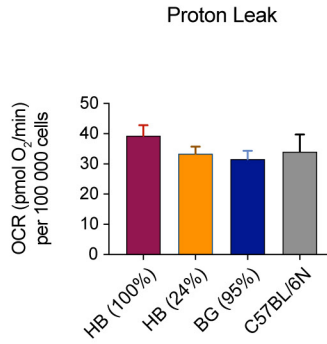
c



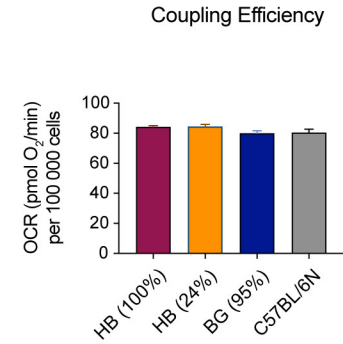
d



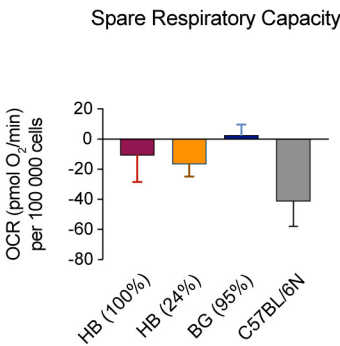
e



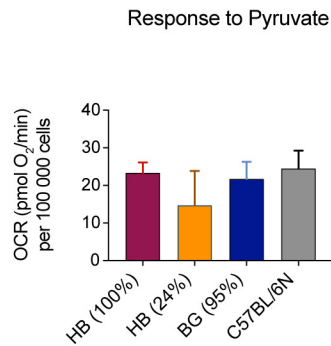
f



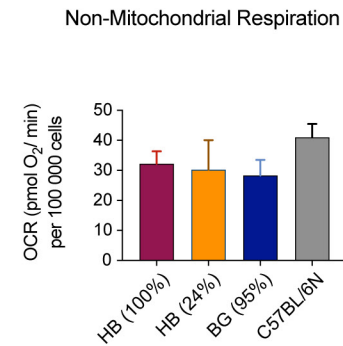
g



h



i

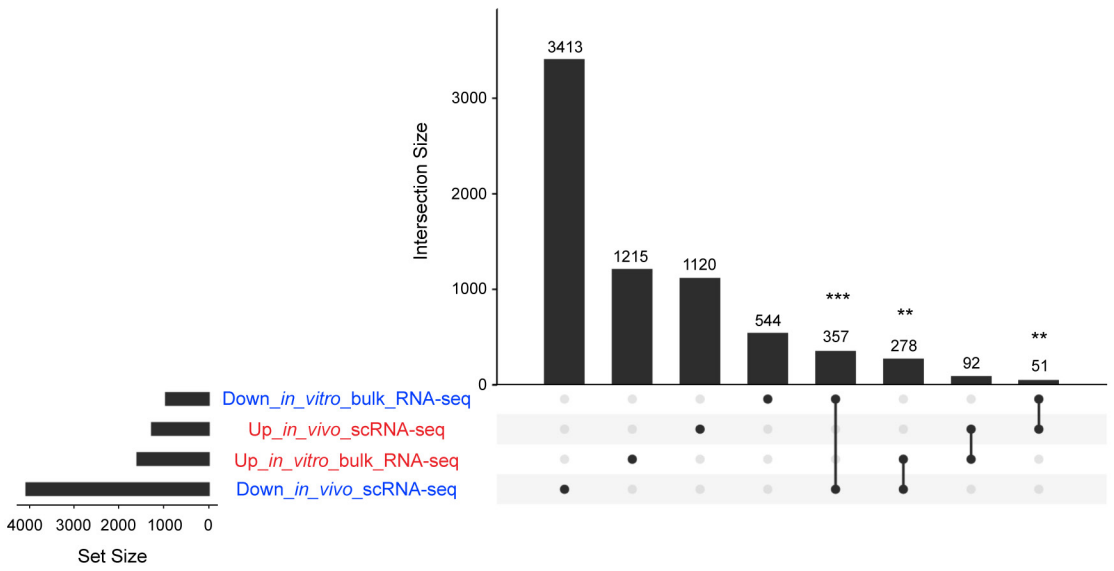


Extended Data Fig. 10

a

Source	Term	Adjusted p-value
GO:CC	mitochondrial protein complex	5.91E-05
GO:CC	inner mitochondrial membrane protein complex	8.84E-04
GO:CC	mitochondrial inner membrane	8.93E-04
GO:CC	mitochondrial respirasome	2.44E-03
GO:CC	respiratory chain complex	3.89E-03
GO:CC	respirasome	6.50E-03
GO:CC	mitochondrial part	1.06E-02
GO:CC	organelle inner membrane	4.65E-02
KEGG	oxidative phosphorylation	7.71E-04
KEGG	Huntington disease	2.35E-03
WP	electron transport chain	1.26E-03

b



c

